

IN SILICO AND IN VITRO SCREENING OF NEWLY DESIGNED COMPOUNDS AGAINST
COXSACKIVIRUS A16 AND ENTEROVIRUS A71



A Thesis Submitted in Partial Fulfillment of the Requirements
for the Degree of Master of Science in Biochemistry and Molecular Biology

Department of Biochemistry

FACULTY OF SCIENCE

Chulalongkorn University

Academic Year 2021

Copyright of Chulalongkorn University

การคัดกรองเชิงคอมพิวเตอร์และในระดับหลอดทดลองของสารออกแบบใหม่ที่มีผลต่อคอกซากีไวรัส
เอ16 และเอนเทอโรไวรัส เอ71



วิทยานิพนธ์นี้เป็นส่วนหนึ่งของการศึกษาตามหลักสูตรปริญญาวิทยาศาสตรมหาบัณฑิต
สาขาวิชาชีวเคมีและชีววิทยาโมเลกุล ภาควิชาชีวเคมี
คณะวิทยาศาสตร์ จุฬาลงกรณ์มหาวิทยาลัย
ปีการศึกษา 2564
ลิขสิทธิ์ของจุฬาลงกรณ์มหาวิทยาลัย

Thesis Title *IN SILICO AND IN VITRO* SCREENING OF NEWLY DESIGNED
COMPOUNDS AGAINST COXSACKIVIRUS A16 AND
ENTEROVIRUS A71

By Miss Amita Sripattaraphan

Field of Study Biochemistry and Molecular Biology

Thesis Advisor Associate Professor THANYADA RUNGROTMONGKOL,
Ph.D.

Thesis Co Advisor Assistant Professor SIWAPORN BOONYASUPPAYAKORN,
Ph.D.

Accepted by the FACULTY OF SCIENCE, Chulalongkorn University in Partial
Fulfillment of the Requirement for the Master of Science

..... Dean of the FACULTY OF SCIENCE
(Professor POLKIT SANGVANICH, Ph.D.)

THESIS COMMITTEE

..... Chairman
(Associate Professor KUAKARUN KRUSONG, Ph.D.)

..... Thesis Advisor
(Associate Professor THANYADA RUNGROTMONGKOL,
Ph.D.)

..... Thesis Co-Advisor
(Assistant Professor SIWAPORN BOONYASUPPAYAKORN,
Ph.D.)

..... Examiner
(Assistant Professor Rath Pichyangkura, Ph.D.)

..... External Examiner
(Assistant Professor Jundee Rabablert, Ph.D.)

อมิตา ศรีภัทรพานธุ์ : การคัดกรองเชิงคอมพิวเตอร์และในระดับหลอดทดลองของสารออกแบบใหม่ที่มีผลต่อคอซากกีไวรัส เอ16 และเอนเทอโรไวรัส เอ71. (*IN SILICO AND IN VITRO SCREENING OF NEWLY DESIGNED COMPOUNDS AGAINST COXSACKIVIRUS A16 AND ENTEROVIRUS A71*) อ.ที่ปรึกษาหลัก : รศ. ดร.ธัญญดา รุ่งโรจน์มงคล, อ.ที่ปรึกษาร่วม : ผศ. ดร.ศิวะพร บุญทรัพย์การ

โรคมือเท้าปากเกิดการระบาดขึ้นทั่วโลกจากเชื้อคอซากกีไวรัส เอ16 (CV-A16) และเอนเทอโรไวรัส เอ71 (EV-A71) ซึ่งจัดอยู่ในวงศ์ *Picornaviridae* สกุล *Enterovirus* ในปัจจุบันการรักษาโรคมือเท้าปากทำได้เพียงการรักษาตามอาการ โดยทั่วไปจะเป็นการรักษาเพื่อบรรเทาอาการที่เกิดขึ้นต่าง ๆ แต่ยังไม่มียาต้านไวรัสชนิดนี้โดยเฉพาะ รูพินทรีเวียร์ (AG7088) เป็นตัวยับยั้งชนิดหนึ่งที่ถูกออกแบบขึ้นและมีการรายงานว่าสามารถยับยั้งการทำงานของไวรัสโรคมือเท้าปากและอีกทั้งยังได้รับความสนใจในการพัฒนาอนุพันธ์เพื่อประสิทธิภาพที่ดีขึ้นอีกด้วย รูพินทรีเวียร์เป็นตัวยับยั้งการทำงานของ 3C protease ของไวรัส CV-A16 และ EV-A71 ซึ่งเป็นโปรตีนที่มีความสำคัญในกระบวนการเพิ่มจำนวนของไวรัสชนิดนี้ งานวิจัยนี้ได้ทำการออกแบบอนุพันธ์รูพินทรีเวียร์จำนวน 50 ตัว โดยทำการเปลี่ยนหมู่ฟังก์ชันของรูพินทรีเวียร์ในตำแหน่ง P1', P1, P2, P3 และ P4 โดยวิธีการทางคอมพิวเตอร์ หลังจากทำการคำนวณประสิทธิภาพการจับกับโปรตีนของอนุพันธ์แต่ละตัว พบอนุพันธ์ 5 ตัวที่มีประสิทธิภาพการจับกับโปรตีนดีกว่ารูพินทรีเวียร์ ได้แก่ P1'-1, P2-m3, P3-4, P4-5, และ P4-19 นอกจากนี้ยังใช้วิธีการจำลองพลวัตเชิงโมเลกุล เป็นเวลา 500 นาโนวินาที (ns) เพื่อศึกษาสมบัติทางโครงสร้าง สมบัติพลวัต และสมบัติทางเทอร์โมไดนามิกส์ของโปรตีน การศึกษาพบว่า อนุพันธ์ P2-m3 ที่ประกอบด้วย meta-aminomethyl-benzyl ที่ตำแหน่ง P2 ได้แสดงประสิทธิภาพในการจับกับโปรตีน 3Cpro ได้ดีที่สุด โดย P2-m3 มีจำนวนพันธะไฮโดรเจนและ จำนวนอะตอมล้อมรอบระหว่างอนุพันธ์และโปรตีนมากที่สุด อีกทั้ง P2-m3 สร้างพันธะไฮโดรเจนระหว่างกรดอะมิโน L127 และ K130 ที่ตำแหน่ง P2 ซึ่งเป็นพันธะที่แข็งแรงกว่าในรูพินทรีเวียร์ นอกจากนี้ P2-m3 ยังแสดงค่าพลังงานเสรีของการยึดจับน้อยที่สุดอีกด้วย P2-m3 จึงเป็นอนุพันธ์ที่ควรทำการสังเคราะห์และทดสอบประสิทธิภาพระดับเซลล์ต่อไป นอกจากนี้ผู้วิจัยยังพบสารประกอบฟลาโวนอยด์ที่มีประสิทธิภาพในการยับยั้งไวรัสโรคมือเท้าปากจากการศึกษาด้วยวิธี pharmacophore-based virtual screening. จากการศึกษพบว่า สารประกอบฟลาโวนอยด์ทั้ง 39 ตัวพบสารประกอบ 3 ตัวที่มีประสิทธิภาพการจับกับโปรตีน 3Cpro ของ CV-A16 และ EV-A71 ได้ดี ได้แก่ diosmin, epigallocatechin gallate (EGCG), และ RTH-011 นอกจากนี้ยังพบว่าสารประกอบ EGCG แสดงค่า EC_{50} สำหรับการยับยั้ง EV-A71 และ CV-A16 เท่ากับ $12.86 \pm 1.30 \mu\text{M}$ และ $15.54 \pm 1.50 \mu\text{M}$ ตามลำดับ ในขณะที่ diosmin แสดงค่า EC_{50} สำหรับการยับยั้ง EV-A71 และ CV-A16 เท่ากับ $21.01 \pm 1.57 \mu\text{M}$ และ $30.68 \pm 3.25 \mu\text{M}$ ตามลำดับ สารประกอบทั้งสอง ไม่พบความเป็นพิษต่อเซลล์ RD โดย EGCG และ diosmin แสดงค่า CC_{50} มากกว่า 250 และ 500 μM ตามลำดับ ผลการศึกษาด้วยวิธีการจำลองพลวัตเชิงโมเลกุล ยังแสดงให้เห็นว่า EGCG มีประสิทธิภาพการจับกับโปรตีนได้ดีกว่า โดย EGCG แสดงค่าพลังงานเสรีของการยึดจับน้อยกว่าและมีจำนวนอะตอมล้อมรอบมากกว่า diosmin ซึ่งสอดคล้องกับผลของการวิเคราะห์กรดอะมิโนที่สำคัญต่อการยึดจับ พบว่า EGCG มีตำแหน่งของกรดอะมิโนที่สำคัญ คล้ายคลึงกับรูพินทรีเวียร์มากกว่า diosmin งานวิจัยนี้พบว่า EGCG เป็นสารประกอบที่มีประสิทธิภาพในการยับยั้งโปรตีน 3Cpro ของ EV-A71 และ CV-A16 และเหมาะแก่การนำไปพัฒนาเป็นยาสำหรับโรคมือเท้าปากต่อไป

สาขาวิชา ชีวเคมีและชีววิทยาโมเลกุล

ปีการศึกษา 2564

ลายมือชื่อนิสิต

ลายมือชื่อ อ.ที่ปรึกษาหลัก

ลายมือชื่อ อ.ที่ปรึกษาร่วม

6172152323 : MAJOR BIOCHEMISTRY AND MOLECULAR BIOLOGY

KEYWORD: Hand foot and mouth disease, Coxsackievirus A16, Enterovirus A71

Amita Sripattaraphan : *IN SILICO* AND *IN VITRO* SCREENING OF NEWLY DESIGNED COMPOUNDS AGAINST COXSACKIVIRUS A16 AND ENTEROVIRUS A71. Advisor: Assoc. Prof. THANYADA RUNGROTMONGKOL, Ph.D. Co-advisor: Asst. Prof. SIWAPORN BOONYASUPPAYAKORN, Ph.D.

Outbreaks of hand, foot, and mouth disease (HFMD) occur around the world. It is caused by the Coxsackievirus-A16 (CV-A16) and Enterovirus-A71 (EV-A71) that belong to the *Enterovirus* genus. Unfortunately, neither an anti-HFMD drug nor a vaccine is currently available. Rupintrivir, one of the drug candidates for HFMD treatment, has been attractive for the development of its analogs with broad biological activities. This drug is an inhibitor for 3C protease of CV-A16 and EV-A71, an enzyme that plays a crucial role in the viral replication process. In the present study, we focused on designing 50 novel rupintrivir analogs against CV-A16 and EV-A71 3Cpro using computational tools. From their predicted binding affinities, the five compounds with functional group modifications at P1', P2, P3, and P4 sites, namely P1'-1, P2-m3, P3-4, P4-5, and P4-19, could bind with both CV-A16 and EV-A71 3Cpro better than rupintrivir. Subsequently, these five analogs were studied by 500 ns molecular dynamics simulations. Among them, P2-m3, the derivative with meta-aminomethyl-benzyl group at the P2 site, showed the greatest potential to interact with the 3Cpro target by delivering the highest number of inter-molecular hydrogen bonds and contact atoms. It formed the hydrogen bonds with L127 and K130 residues at the P2 site stronger than rupintrivir, supported by significantly lower MM/PB(GB)SA binding free energies. The P2-m3 was suggested to be synthesized and tested the biological activity. Moreover, we found new potential compounds against 3C protease of EV-A71 and CV-A16 from flavonoids by using pharmacophore-based virtual screening. Among 39 flavonoids, diosmin, epigallocatechin gallate, EGCG, and RTH-011 showed high binding affinity against EV-A71 and CV-A16. In addition, we found that EGCG showed the highest potent efficacy (EC_{50}) at the values of $12.86 \pm 1.30 \mu\text{M}$ and $15.54 \pm 1.50 \mu\text{M}$ for EV-A71 and CV-A16, respectively, while diosmin showed EC_{50} at the values of $21.01 \pm 1.57 \mu\text{M}$ and $30.68 \pm 3.25 \mu\text{M}$ for EV-A71 and CV-A16, respectively. Both compounds no toxic ($CC_{50} > 250 \mu\text{M}$ and $> 500 \mu\text{M}$ for EGCG and diosmin, respectively) against RD cells were obtained. Moreover, the MD simulation analysis revealed that EGCG had higher the binding affinity than diosmin supported by significantly lower SIE binding free energies, higher number contact atom and higher number of key binding residue which similar to rupintrivir. We suggested that the EGCG compounds are effective in inhibiting EV-A71 and CV-A16 3C protease.

Field of Study:	Biochemistry and Molecular Biology	Student's Signature
Academic Year:	2021	Advisor's Signature
		Co-advisor's Signature

ACKNOWLEDGEMENTS

First and foremost, I would like to thank my thesis advisor Associate Professor Dr. Thanyada Rungrotmongkol, who always guided me in doing the thesis. She provided us with invaluable advice and helped us in difficult periods. Her motivation and help contributed tremendously to the successful completion of the thesis. I would also like to greatly thank my co-advisor, Associate Professor Siwaporn Boonyasuppayakorn for her mentorship and helpful commentary of this research, especially in the experimental investigations.

My gratitude is also extended to the chairman and thesis committees, Associate Professor Dr. Teerapong Buaboocha, Assistant Professor Rath Pichyangkura, and Assistant Professor Jundee Rabablert for their useful guidance and constructive criticism throughout my study.

I also thank the Structural and Computational Biology Research Group and Computational Chemistry Unit Cell. Sincere thanks are expressed to all members of Biosim Lab, especially Dr. Kamonpan Sanachai, Miss. Thitinan Aiebchun and Virology lab member, especially Miss. Benyapa Kaewmalai from Department of Microbiology, Faculty of Medicine, Chulalongkorn University for their technical assistance and helpful encouragement.

Finally, I would like to thank the Development and Promotion of Science and Technology Talents Project (DPST) for scholarship, and the 90th Anniversary of Chulalongkorn University Fund (Ratchadaphisaksomphot Endowment Fund, GCUGR1125633083M).

Amita Sripattaraphan

TABLE OF CONTENTS

	Page
.....	iii
ABSTRACT (THAI).....	iii
.....	iv
ABSTRACT (ENGLISH).....	iv
ACKNOWLEDGEMENTS.....	v
TABLE OF CONTENTS.....	vi
LIST OF TABLES.....	ix
LIST OF FIGURES.....	x
LIST OF PUBLICATION.....	1
INTRODUCTION.....	2
1.1 Research concept.....	2
1.2 Research rationality.....	2
1.3 Research objectives.....	4
1.4 Scope of the research.....	5
1.5 Expected beneficial outcome(s) from the thesis.....	5
CHAPTER I.....	6
MANUSCRIPT I.....	6
1. Introduction.....	9
2. Material and methods.....	11
2.1. System Preparation and Compound Screening.....	11
2.2. Molecular Dynamics Simulations.....	12

3. Results and Discussion	13
3.1. Rational Design and Screening	13
3.2. Stability of the Simulated Complexes.....	15
3.3. Number of Contact Atoms and H-Bonds	16
3.4. Key Binding Residues.....	19
3.5. Predicted Binding Affinity of the Potent Rupintrivir Analog	21
4. Conclusions	22
Acknowledgment.....	22
CHAPTER II.....	23
MANUSCRIPT II	23
1. Introduction.....	26
2. Material and Methods	29
2.1. Pharmacophore modeling	29
2.1.1 Pharmacophore modeling.....	29
2.1.2. Virtual screening	29
2.1.3. Model validation	30
2.1.4. Molecular Docking.....	30
2.2.1. Cells and viruses.....	31
2.2.2. Cytotoxicity study.....	31
2.2.3. Antiviral efficacy of selected compounds.....	31
2.3. Molecular dynamic simulation.....	32
3. Results and Discussion	33
3.1 Pharmacophore models and virtual screening.....	33
3.2 Virtual Screening Validation	34

3.3 Molecular docking of potent compounds.....	36
3.4 Cytotoxicity and Inhibitory effect of the potent compound.....	40
3.5 Mechanism of potent compounds binding.....	41
4. Conclusions	47
APPENDIX.....	49
REFERENCES	63
VITA.....	72



LIST OF TABLES

	Page
<i>Table 1</i> Relative interaction energy ($\Delta\Delta G_{\text{residue, bind}}$) of the designed compounds in comparison to rupintrivir against EV-A71 3Cpro derived from MM/PBSA and MM/GBSA methods ($\Delta G_{\text{rupintrivir, bind}}$ of -19.38 and -32.83 kcal/mol, respectively). The compounds with negative $\Delta\Delta G_{\text{bind}}$ are in bold, and their 2D structures are given in Figure 2.	14
<i>Table 2</i> Number of contact atoms within the 3.5-Å sphere of the focused compounds for CV-A16 and EV-A71 3Cpro systems taken from the last 50 ns of three independent simulations. The analog with bold was a potent compound.	17
<i>Table 3</i> Number of hydrogen bonds of the focused compounds with CV-A16 and EV-A71 3Cpro calculated from the last 50 ns of the three independent simulations.	17
<i>Table 4</i> List of hit compounds, pharmacophore fit score and fitness score against EV-A71 and CV-A16	35
<i>Table 5</i> The energy components (kcal/mol) of potent compounds/3Cpro calculated with the SIE method	44

LIST OF FIGURES

	Page
<i>Figure 1</i> (A) The 3D structure of EV-A71 3Cpro in complex with rupintrivir (PDB ID: 3R0F) [27] (ball and stick green model), where the catalytic triad are shown in blue stick model. (B) The chemical structure of rupintrivir.....	11
<i>Figure 2</i> The chemical structure of five selected compounds with $\Delta\Delta G_{\text{bind}} < 0$ kcal/mol	15
<i>Figure 3</i> All-atom RMSD plots for the CV-A16 and EV-A71 3Cpro in complex with five focused analogs P4-5, P4-19, P1'-1, P2-m3, and P3-4, as well as rupintrivir, plotted along the 500 ns from the three independent simulations (Run1, Run2, and Run3)..	16
<i>Figure 4</i> Percentage of intermolecular H-bond occupation with P1, P2, and P3 sites of the rupintrivir and its analog P2-m3 with EV-A71 and CV-A16 3Cpro derived from the last 50 ns simulations, where the representative structures are depicted in Figure 5. Only H-bond occupation >40% is shown in the histogram.	18
<i>Figure 5</i> Hydrogen bonding interactions of the rupintrivir and its analog P2-m3 (bond and stick model) with EV-A71 and CV-A16 3Cpro residues (stick model).	19
<i>Figure 6</i> MM-PBSA per-residue decomposition free energy of the rupintrivir and its analog P2-m3 in complex with EV-A71 and CV-A16 3Cpro.	20
<i>Figure 7</i> The contributing residues involved in ligand binding are colored according to the per-residue decomposition free energy ($\Delta G_{\text{residue, bind}}$), where the highest to lowest free energies are shaded from white to blue.	20
<i>Figure 8</i> (A) The molecular mechanical energy (ΔE_{MM}) including electrostatic (ΔE_{ele}) and van der Waals (ΔE_{vdw}) interactions and (B) binding free energy (ΔG_{bind}) based on the MM/PBSA method for rupintrivir and P2-m3 binding to EV-A71 and CV-A16 3Cpro.	21
<i>Figure 9</i> The superimposition structure of EV-A71 (PDB ID: 3R0F) and CV-A16 (PDB ID: 3SJI) in complex with rupintrivir (ball and stick model).	28

<i>Figure 10</i> The workflow of this work for searching a newly potent compound against EV-A71 and CV-A16.....	28
<i>Figure 11</i> The 2D and 3D pharmacophore models of the rupintrivir/EV-A71 and CV-A16 3C protease complexes and the interacting residues extracted from the first snapshot of the last 50 ns MD trajectories. The pharmacophore features are represented as green arrows (HBD), red arrows (HBA), and yellow spheres (hydrophobic property). The interaction with the percentage greater than 30% were labeled and considered to be the main interaction for binding.....	34
<i>Figure 12</i> Receiver operating characteristic (ROC) plot of pharmacophore model applied to EV-A71 and CV-A16 3C protease. The area under the curve (AUC) is given for 1, 5, 10, and 100% of the database.....	36
<i>Figure 13</i> The potent compounds were docked into the active site of EV-A71 and CV-A16 3Cpro which has rupintrivir as a reference drug.....	38
<i>Figure 14</i> The 2D interactions of potent compounds and rupintrivir in EV-A71 and CV-A16 3Cpro complexes. The residues with black label were substrate binding residues while the residues with red label were critical binding residues.....	39
<i>Figure 15</i> Cytotoxicity of diosmin and EGCG against RD cells using MTS assay. The compounds were dissolved in DMSO and diluted into eight concentrations (1, 5, 10, 25, 50, 100, 250, and 500 μ M).....	41
<i>Figure 16</i> Inhibitory activity of diosmin and EGCG toward RD cell infection by EV-A71 and CV-A16.....	41
<i>Figure 17</i> A) All-atom RMSD (500ns MD simulation), B) number of contacts atom, and number of H-bonds of diosmin and EGCG in complex with EV-A71 3Cpro plotted along the last 50 ns MD simulation. The percentages of hydrogen bond occupation are shown in D).....	43
<i>Figure 18</i> MM-PBSA per-residue decomposition free energy of the diosmin and EGCG in complex with EV-A71 3Cpro. The contributing residues involved in ligand binding	

are colored according to the per-residue decomposition free energy ($\Delta G_{\text{residue, bind}}$), where the highest to lowest free energies are shaded from blue to yellow..... 44

Figure 19 A) PCA scree plot of PC modes and B) the 2D projection of first two PC modes, derived from MD trajectories of the EV-A71 3Cprotease apo form and holo form with diosmin and EGCG..... 46

Figure 20 The porcupine plots corresponding to PC1 obtained from PCA analysis of apo form and holo form with diosmin and EGCG/EV-A71 3Cpro. The head of the arrow (yellow) represents the direction of motion, while its length represents the amplitude of the protein motion..... 47



LIST OF PUBLICATION

This thesis contains general summary (introduction, some background information and conclusion) and the following paper which are referred to in the text by their roman number.

Manuscript I: Computational Screening of Newly Designed Compounds Against Coxsackievirus A16 and Enterovirus A71

Manuscript II: Discovery of potent compounds for active against coxsackievirus A16 and enterovirus A71 by virtual screening



INTRODUCTION

1.1 Research concept

Hand Foot and Mouth disease is caused by a virus. Coxsackievirus A16 (CV-A16) and Enterovirus A71 (EV-A) [1]. It is easily transmitted by direct contact through excretion, saliva, and fecal matter [2]; thus, the number of people infected with HFMD has increased almost every year, particularly children under five years old. The 3C protease of CV-A16 and EV-A71, an enzyme that plays a crucial role in the viral replication process. Rupintrivir, one of the drug candidates for HFMD treatment, has been attractive for the development of its analogs with broad biological activities [3]. We aimed to search for the new potent compounds against the 3C protease of CV-A16 and EV-A71. For the development process, the cost and time consumption in high throughput screening for hit (lead) compounds is generally expensive; however, it can be reduced by applying high-performance computational techniques. Moreover, the cell-based assay was performed to investigate the biological activity of the potent compound for inhibiting the CV-A16 and EV-A71.

1.2 Research rationality

Enterovirus A71 (EV-A71) and coxsackievirus A16 (CV-A16) are single-stranded, viruses-sense RNA virus belonging to the Enterovirus genus of *Picornavirales* order. This disease has spread in several Asian-pacific countries, including Australia, Cambodia, China, Japan, Malaysia, Taiwan, Vietnam, and Thailand [1]. It is easily transmitted by direct contact through excretion, saliva, and fecal matter[2, 3]; thus, the number of people infected with HFMD has increased almost every year, particularly children under five years old [4-6]. Most of the patients have a mild, fever, rashes on hands and feet, and mouth [7]. A small proportion of infected children may rapidly develop severe and even fatal neurological and systemic complications [8]. The genome of enteroviruses contains a positive single-strand RNA (ssRNA) with a single open reading frame (ORF) encoding a large polyprotein

precursor that requires proteolytic processing to produce viral structural and replication proteins. After the virus enters the host cells, a viral polyprotein is produced and further cleaved into the four structural proteins (Vp1, Vp2, Vp3, and Vp4) and seven non-structural proteins (2A, 2B, 2C, 3A, 3B, 3C, and 3D) by the activity of 3C proteases (3Cpro) [2]. The 3Cpro is a cysteine protease that favorably cleaves the peptide bond between glutamine (Q) and glycine (G) of viral protein through a reaction involved in catalytic triad residues (H40, E71, and C147) [9]. 3C protease similar to the 2A protease, the EV-A71 3C protease also plays a role to cleave the eukaryotic initiation factor 4A (eIF4A) 141 and eukaryotic initiation factor 5B (eIF5B) of the host cap-dependent translation [10].

Therefore, the primary roles of 3Cpro in the life cycle of EV-A71 and CV-A16 make it an ideal drug target against CV-A16 and EV-A71 viruses [11]. The antiviral drug candidate rupintrivir (AG7088), is a potent peptidomimetic inhibitor of human rhinovirus (HRV) 3C protease. Moreover, rupintrivir also shows a broad-spectrum antibiotic against other members of the family Picornaviridae [12] and is currently proven to be the most effective peptidomimetic 3Cpro inhibitor with a half-maximal inhibitory concentration (IC_{50}) of 2.1 nM against CV-A16 [11, 13]. According to the study of Wang et al. (2017), N69 residue in active site has been reported to stabilize the S2 pocket of EV-A71 3Cpro by forming a hydrogen bond with N atoms of L70 and E70 residues. The mutation of N69 abolishes the bond network by destabilizing the S2 pocket. Thus, a natural substrate binding to EV-A71 3Cpro can possibly occur in the presence of an inhibitor. They suggested that it is conceivable that modification of the P2 residue with a longer side chain can increase the inhibitory effect [14]. In this work, the interaction energy prediction and all-atom molecular dynamics (MD) simulation [15] were employed to screen a series of the designed rupintrivir analogs against 3Cpro of CV-A16 and EV-A71.

Moreover, most of studies see the importance of natural compounds. Flavonoids is the one of the most natural compounds which is studied the activity. Flavonoids are naturally polyphenolic compounds widely distributed in plants and are effective for a wide variety of biological functions [16]. They have become compounds of interest for natural drug discovery research. Flavonoids have several

pharmacological properties including antioxidant, anti-inflammatory, anticancer, and antiviral [17]. Many studies reported about the antiviral efficiency of flavonoids. Quercetin catechin and naringenin demonstrated strong inhibition of hepatitis C virus (HCV) infectious [18]. Epigallocatechin gallate (EGCG), the main constituent of green tea, has been reported to block HIV-1 replication before its integration into host DNA [19]. Another study reported that baicalin interferes the intracellular virus replication, inactivate the free DENV particles and affects viral attachment step of DENV to host cells [20]. Moreover, diosmin is a chemical in citrus fruits. It has been reported about blocking the coronavirus to enter the host cells [21].

Nowadays, several computational techniques have become the most effective methods in drug discovery and development. A pharmacophore-based screening approach is one of the most advantageous tools for the fast and accurate virtual screening of databases with millions of compounds that match the similarity of the three-dimensional (3D) interaction pattern or pharmacophore model of drug-like compounds with known ligands in the complexes [22-25]. Therefore, we aimed to find new potential compounds against 3C protease of EV-A71 and CV-A16 from flavonoids by using pharmacophore-based virtual screening. Subsequently, molecular docking was used to study the binding interactions at the atomic level of potent compounds with 3C protease of EV-A71 and CV-A16. Finally, the cytotoxicity and antiviral efficacy against EV-A71 and CV-A16 infection in human rhabdomyosarcoma (RD) cells of potent compounds were also performed.

1.3 Research objectives

- i) To design and search the potent compound against the CV-A16 and EV-A71 3Cpro by computational screening
- ii) To search new potential compounds against 3C protease of EV-A71 and CV-A16 from flavonoids by using pharmacophore-based virtual screening

1.4 Scope of the research

- i) The rupintrivir was used to be a reference drug for study the efficiency of potent compound.
- ii) The potent compound was studied the biology activity by cell-based assay
- iii) The potent compound was investigated the binding behavior by MD simulations.

1.5 Expected beneficial outcome(s) from the thesis

This study obtains the newly potent compound that could inhibit 3Cpro of CV-A16 and EV-A71, which may be useful to develop as novel anti-HFMD.



CHAPTER I
MANUSCRIPT I

Computational Screening of Newly Designed Compounds Against Coxsackievirus
A16 and Enterovirus A71

Amita Sripattaraphan¹, Kamonpan Sanachai¹, Warinthorn Chavasiri², Siwaporn Boonyasuppayakorn³ Phorn-phimon Maitarad⁴ and Thanyada Rungrotmongkol^{1,5, *}

¹ Structural and Computational Biology Research Unit, Department of Biochemistry, Faculty of Science, Chulalongkorn University, Bangkok, Thailand; bbeeamita@gmail.com (A.S.); sanachaikamonpan@gmail.com (K.S.)

² Department of Chemistry, Faculty of Science, Chulalongkorn University, Bangkok 10330, Thailand; warinthorn.c@chula.ac.th

³ Applied Medical Virology Research Unit, Department of Microbiology, Faculty of Medicine, Chulalongkorn University, Bangkok 10330, Thailand; siwaporn.b@chula.ac.th

⁴ Research Center of Nano Science and Technology, Shanghai University, Shanghai 200444, PR; pmaitarad@shu.edu.cn

⁵ Ph.D. Program in Bioinformatics and Computational Biology, Graduate School, Chulalongkorn University, Bangkok 10330, Thailand

* Correspondence: thanyada.r@chula.ac.th, t.rungrotmongkol@gmail.com

This article has been published in *Molecules*

Computational Screening of Newly Designed Compounds Against Coxsackievirus A16 and Enterovirus A71

Amita Sripattaraphan¹, Kamonpan Sanachai¹, Warinthorn Chavasiri², Siwaporn Boonyasuppayakorn³ Phorn-phimon Maitarad⁴ and Thanyada Rungrotmongkol^{1,5, *}

¹ Structural and Computational Biology Research Unit, Department of Biochemistry, Faculty of Science, Chulalongkorn University, Bangkok, Thailand; bbeamita@gmail.com (A.S.); sanachaikamonpan@gmail.com (K.S.)

² Department of Chemistry, Faculty of Science, Chulalongkorn University, Bangkok 10330, Thailand; warinthorn.c@chula.ac.th

³ Applied Medical Virology Research Unit, Department of Microbiology, Faculty of Medicine, Chulalongkorn University, Bangkok 10330, Thailand; siwaporn.b@chula.ac.th

⁴ Research Center of Nano Science and Technology, Shanghai University, Shanghai 200444, PR; pmaitarad@shu.edu.cn

⁵ Ph.D. Program in Bioinformatics and Computational Biology, Graduate School, Chulalongkorn University, Bangkok 10330, Thailand

* Correspondence: thanyada.r@chula.ac.th, t.rungrotmongkol@gmail.com

This article has been published in **Molecules**

CHULALONGKORN UNIVERSITY

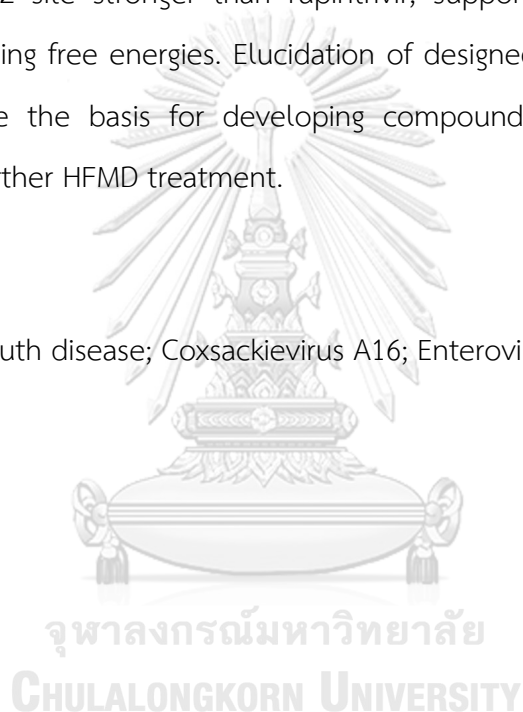
Abstract

Outbreaks of hand, foot, and mouth disease (HFMD) that occurred worldwide are mainly caused by the Coxsackievirus-A16 (CV-A16) and Enterovirus-A71 (EV-A71). Unfortunately, neither an anti-HFMD drug nor a vaccine is currently available. Rupintrivir in phase II clinical trial candidate for rhinovirus showed highly potent antiviral activities against enteroviruses as an inhibitor for 3C protease (3Cpro). In the present study, we focused on designing 50 novel rupintrivir analogs against CV-A16 and EV-A71 3Cpro using computational tools. From their predicted binding affinities,

the five compounds with functional group modifications at P1', P2, P3, and P4 sites, namely P1'-1, P2-m3, P3-4, P4-5, and P4-19, could bind with both CV-A16 and EV-A71 3Cpro better than rupintrivir. Subsequently, these five analogs were studied by 500-ns molecular dynamics simulations. Among them, P2-m3, the derivative with meta-aminomethyl-benzyl group at the P2 site, showed the greatest potentials to interact with the 3Cpro target by delivering the highest number of intermolecular hydrogen bonds and contact atoms. It formed the hydrogen bonds with L127 and K130 residues at the P2 site stronger than rupintrivir, supported by significantly lower MM/PB(GB)SA binding free energies. Elucidation of designed rupintrivir analogs in our study will provide the basis for developing compounds that can be candidate compounds for further HFMD treatment.

Keywords

Hand foot and mouth disease; Coxsackievirus A16; Enterovirus A71; 3C protease; in silico drug design



1. Introduction

Hand Foot and Mouth Disease (HFMD) is one of the global public health concerns that are widely spread worldwide, especially in the southeast pacific region, e.g., China [26], Japan [27], Taiwan [28], Singapore [29], and Thailand [30]. It is easily transmitted by direct contact through excretion, saliva, and fecal matter [3]; thus, the number of people infected with HFMD has increased almost every year, particularly children under five years old [4-6]. HFMD is generally associated with the viral infection of coxsackievirus A16 (CV-A16) and enterovirus A71 (EV-A71), which belong to the Enterovirus genus of *Picornavirales* order [29]. Moreover, the EV-A71 strongly correlated with the more severe clinical outcome, especially in neurological sequelae such as encephalitis and meningitis [31, 32]. The genome of enteroviruses contains a positive single-strand RNA (ssRNA) with a single open reading frame (ORF) encoding a large polyprotein precursor that requires proteolytic processing to produce viral structural and replication proteins. After the virus enters the host cells, a viral polyprotein is produced and further cleaved into the four structural proteins (Vp1, Vp2, Vp3, and Vp4) and seven non-structural proteins (2A, 2B, 2C, 3A, 3B, 3C, and 3D) by the activity of viral and host proteases [2]. The 3C cysteine protease (3Cpro, **Figure 1A**) favorably cleaves the scissile peptide bond between glutamine (Q) and glycine (G) through its catalytic residues (H40, E71, and C147) during the viral replication process. In addition, the EV-A71 3Cpro facilitates progeny virus production and helps the virus evade host antiviral immunity by inter-action with the cleavage of host factors [11]. Therefore, the primary roles of 3Cpro in the life cycle of EV-A71 and CV-A16 make it an ideal drug target against CV-A16 and EV-A71 viruses [2, 11].

Rupintrivir (AG7088, chemical structure in **Figure 1B**) is a drug candidate against the 3Cpro of human rhinovirus (HRV) [2, 11] and is currently proven to be the most effective peptidomimetic 3Cpro inhibitor with a half-maximal inhibitory concentration (IC_{50}) of 2.1 nM against CV-A1 [11, 13]. In addition, it displays a broad-spectrum inhibitory activity against other viruses belonging to the Picornaviridae

family, such as CVB2, CVB5, EV6 EV-A71, and EV9 [33, 34]. Its activity significantly decreases in EV-A71 approximately ~100-fold compared to HRV [6, 29, 35]. The rhinovirus inhibition in the phase II clinical trial was stopped because the rupintrivir failed to meet desired clinical parameters [9, 12, 36-39]. Moreover, it was poorly aqueous soluble with low oral bioavailability challenging further pharmacological development [40]. In addition, the synthesized peptidic Michael acceptor compound SG85, is a rupintrivir-modified compound that acts as an inhibitor of EV-A71 3Cpro (EC50 of ~180 nM) [41]. A previous study of molecular dynamics (MD) simulations revealed that SG85 shared a binding pattern against CV-A16 3Cpro similar to the rupintrivir/EV-A71 complex [42]. According to the study of Wang et al. (2017), N69 residue in active site has been reported to stabilize the S2 pocket of EV-A71 3Cpro by forming a hydrogen bond with N atoms of L70 and E70 residues. The mutation of N69 abolishes the bond network by destabilizing the S2 pocket. Thus, a natural substrate binding to EV-A71 3Cpro can possibly occur in the presence of an inhibitor. They suggested that it is conceivable that modification of the P2 residue with a longer side chain can increase the inhibitory effect [14].

For the drug design and development process, the cost and time consumption in high throughput screening for hit (lead) compounds is generally expensive; however, it can be reduced by applying high-performance computational techniques. In this work, the interaction energy prediction and all-atom molecular dynamics (MD) simulation [15] were employed to screen a series of the designed rupintrivir analogs against 3Cpro of CV-A16 and EV-A71. Additionally, detailed knowledge of the binding mechanisms of the most potent compound would be helpful in the development of new anti-HFMD agents.

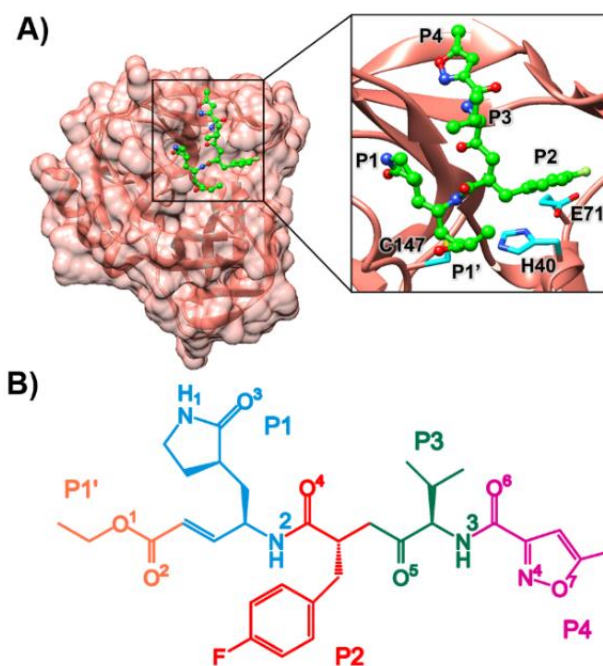


Figure 1 (A) The 3D structure of EV-A71 3Cpro in complex with rupintrivir (PDB ID: 3R0F) [27] (ball and stick green model), where the catalytic triad are shown in blue stick model. (B) The chemical structure of rupintrivir.

2. Material and methods

2.1. System Preparation and Compound Screening

The X-ray crystal structures of rupintrivir in complex with the 3Cpro of CV-A16 and EV-A71 were obtained from Protein Data Bank (PDB), entry codes 3SJI [23] and 3R0F [11], respectively. Note that the CV-A16 and EV-A71 3Cpro share a similar sequence with 91% of identity and 96% of similarity (Figure S3). Based on inhibitor–target interactions in CV-A16/EV-A71 3Cpro complex, the structure-based drug design was used to design the rupintrivir analogs at P1', P1, P2, P3, and P4 sites. To prepare the 3D structures of each designed ligand, their protonation states were then determined using PROPKA 3.1 [43, 44]. The partial atomic charges and empirical force field parameters for each ligand were developed according to the standard procedure [45-47]. The atomic charges of each inhibitor were calculated using HF/6-31G(d) method implemented in the Gaussian09 software [48]. The electrostatic potential (ESP) charges were consequently calculated with the same level of theory

and were then fitted into restrained ESP (RESP) charges using the ANTECHAMBER module of AMBER16 [49, 50]. The FF14SB [51] and GAFF2 [52] force fields were applied for protein and ligands, respectively. All missing hydrogen atoms of protein and ligand were added using the LEaP module and were then minimized to remove the bad contacts. The complexes were solvated in the TIP3P [53, 54] water box with a minimum distance of 10 Å between the protein surface. Afterward, the complexes were energy-minimized by 1500 interactions of steepest descent (SD) and conjugated gradient (CG) methods using AMBER16 with the AMBER ff14SB force field. The binding affinity of all designed analogs toward both 3Cpro enzymes was predicted using MMPB(GB)SA interaction energy calculations. The designed ligands with lower interaction energy than rupintrivir were selected to study the structural dynamics and binding strength within proteins by all-atom molecular dynamics simulations.

2.2. Molecular Dynamics Simulations

The potent ligands from interaction energy screening were simulated under periodic boundary conditions with NPT ensemble. In brief, a residue-based cutoff of 10 Å was employed for nonbonded interactions, and the particle mesh Ewald summation method [15] was used to treat the electrostatic interactions. The SHAKE algorithm [41] was applied to constrain all covalent bonds involving hydrogen atoms. A simulation time step of 2 fs was used along with the MD simulation. The Langevin thermostat [42] with a collision frequency of 2 ps⁻¹ was employed for temperature control, while the Berendsen barostat [14] with a pressure-relaxation time of 1 ps was used to maintain the standard pressure of the system. The simulated models are then heated up to 310 K for 100 ps and are continuously held at this temperature for another 500 ns or until the simulations have reached equilibrium [55], which means the complexes were stable during the simulations. Each complex was simulated three independent MD runs by the difference velocity. Finally, the CPPTRAJ [56] was used to calculate the root-mean-square deviation (RMSD), number of contact atoms, intermolecular hydrogen bonding between ligand/3Cpro. In

addition, the percentage of hydrogen bond occupation, binding pattern, and binding free energy of the most efficient ligand against the two enzymes was further analyzed and compared with rupintrivir.

3. Results and Discussion

3.1. Rational Design and Screening

Based on the inhibitor–ligand interactions of rupintrivir binding to EV-A71 3Cpro in Supplemental **Figure S1**, the 50 analogs were modified using a structure-based drug design as follows. P1 was modified at O³ (e.g., chlorine, fluorine, and methanol) to better interact with K143 in the S1 subsite. P2 was enlarged by the bulkier side chain (e.g., methanamine, ethylamine, and ethanol) to consequently shorten the distance to K130 and Q71 residues in the S2 subsite. To interact with S128 in the S3 subsite, the addition of 2-propanol, 2-fluoropropane, or ammonia was introduced on the side chain of P3. As L125 is located in the S4 subsite, we decided to increase the length of the P4 side chain or to change the functional group (e.g., hydroxyl, methyl, and fluorine). The chemical structures of all 50 compounds are given in **Table S1**.

The previous study reported that EV-A71 was the cause of severe and fatal cases of HFMD (90%), while non-EV-A7 enteroviruses were associated with less than 10% of severe and fatal cases [56]. Therefore, the EV-A71 was used as a reference protein for the initial energy filtering. The MM/PB(GB)SA interaction energy calculations were applied on the minimized complex of analogs/EV-A71 3Cpro. The relative interaction energy of each complex compared to the parent compound rupintrivir ($\Delta\Delta G_{bind} = \Delta G_{bind}^{analog} - \Delta G_{bind}^{rupintrivir}$) is shown in **Table 1**. Among the 50 designed rupintrivir analogs, the five compounds P1'-1, P2-m3, P3-4, P4-5, and P4-19 with negative $\Delta\Delta G_{bind}$ (2D structure shown in **Figure 2**) were selected for investigating the binding pattern and interaction profile in EV-A71 and CV-A16 3Cpro by MD simulations in a further step.

Table 1 Relative interaction energy ($\Delta\Delta G_{\text{residue, bind}}$) of the designed compounds in comparison to rupintrivir against EV-A71 3Cpro derived from MM/PBSA and MM/GBSA methods ($\Delta G_{\text{rupintrivir, bind}}$ of -19.38 and -32.83 kcal/mol, respectively). The compounds with negative $\Delta\Delta G_{\text{bind}}$ are in bold, and their 2D structures are given in **Figure 2**.

Compound	$\Delta\Delta G_{\text{bind}}$ (kcal/mol)		Compound	$\Delta\Delta G_{\text{bind}}$ (kcal/mol)	
	MM/PBSA	MM/GBSA		MM/PBSA	MM/GBSA
P1-1	-9.14	-6.5	P2-m9	0.4	0.94
P1-2	0.17	4.98	P2-m10	3.25	8.96
P1-1	7.82	5.02	P3-1	0.43	3.24
P1-2	20.41	17.58	P3-2	5.67	7.82
P1-3	1.37	1.91	P3-3	2.54	4.15
P1-4	8.28	4.21	P3-4	-4.9	-2.54
P1-5	17.76	14.31	P4-1	1.98	6.27
P2-p1	6.38	5.49	P4-2	1.73	4.25
P2-p2	14.17	14.15	P4-3	2.28	7.36
P2-p3	1.48	2.14	P4-4	12.74	12.79
P2-p4	7.55	9.22	P4-5	-5.34	-5.68
P2-p5	7.85	11.03	P4-6	4.46	2.51
P2-p6	0.73	3.55	P4-7	4.65	4.29
P2-p7	1.37	5.18	P4-8	3.32	2.94
P2-p8	6.65	7.74	P4-9	6.58	4.92
P2-p9	0.65	1.38	P4-10	0.75	1.27
P2-p10	1.56	3.93	P4-11	4.89	3.34
P2-m1	20.47	18.36	P4-12	13.28	11.89
P2-m2	18.59	17.29	P4-13	1.57	0.47
P2-m3	-12.12	-4.2	P4-14	1.64	0.96
P2-m4	2.41	6.29	P4-15	12.68	11.51
P2-m5	8.74	12.38	P4-16	1.55	1.12
P2-m6	1.75	1.35	P4-17	3.03	2.52
P2-m7	0.49	2.03	P4-18	4.12	4.44
P2-m8	1.98	4.71	P4-19	-5.55	-6.68

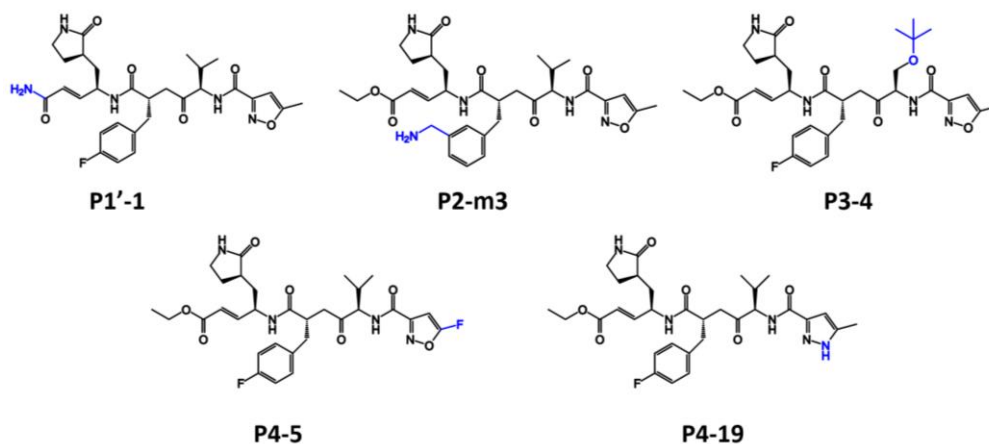


Figure 2 The chemical structure of five selected compounds with $\Delta\Delta G_{\text{bind}} < 0$ kcal/mol

3.2. Stability of the Simulated Complexes

The root mean square displacement (RMSD) of all atoms for each system relative to the minimized structure versus simulation time was measured and plotted in **Figure 3**. The RMSD values of the complexation between rupintrivir or its five analogs and EV-A71/CV-A16 3Cpro from the three independent simulations were about 1.0–2.0 Å from the beginning of simulation until the end. In addition, the superimposition of compounds P1'-1, P2-m3, P3-4, P4-5, P4-19, and rupintrivir against CV-A16 and EV-A71 at the binding site derived from the last 50 ns of simulation in run1 were performed (**Figure S2**). This finding suggested that all ligands were likely stable along with the simulations in the active site. In the study, the last 50 ns of all three simulations were considered for further analyses regarding the number of contact atoms and intermolecular hydrogen bonds between compound and protein targets.

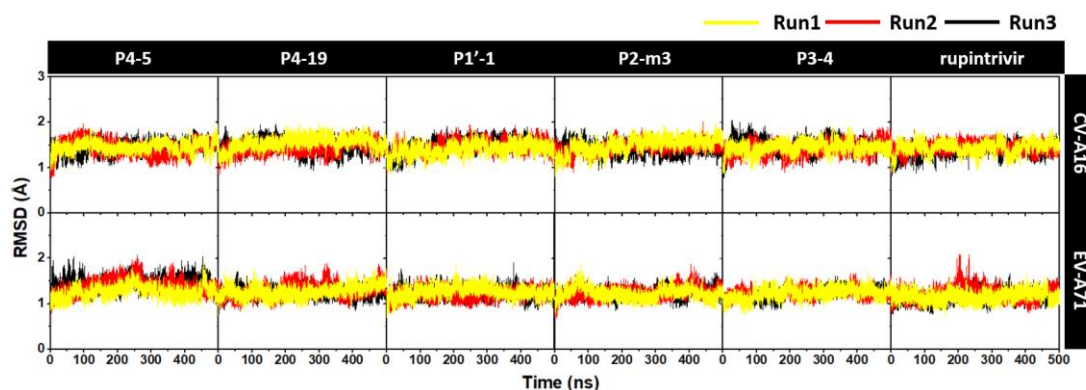


Figure 3 All-atom RMSD plots for the CV-A16 and EV-A71 3Cpro in complex with five focused analogs P4-5, P4-19, P1'-1, P2-m3, and P3-4, as well as rupintrivir, plotted along the 500 ns from the three independent simulations (**Run1, Run2, and Run3**).

3.3. Number of Contact Atoms and H-Bonds

To evaluate the binding strength of the designed compounds in the active site of 3C pro, the number of atom contacts within the 3.5-Å sphere of each analog were counted. The average numbers of contact atoms in the last 50 ns from the three-independent simulation are summarized in **Table 2**. Among five designed analogs, the P2-m3 showed the highest number of contact atoms in both CV-A16 (24.3 ± 4.3) and EV-A71 (22.1 ± 4.5) systems. In addition, this compound gave the number of contact atoms higher than rupintrivir (23.7 ± 4.7 for CV-A16 and 20.0 ± 5.0 systems).

Table 2 Number of contact atoms within the 3.5-Å sphere of the focused compounds for CV-A16 and EV-A71 3Cpro systems taken from the last 50 ns of three independent simulations. The analog with bold was a potent compound.

	CV-A16	EV-A71
P4-5	22.5 ± 5.0	16.1 ± 4.7
P4-19	22.1 ± 5.3	17.4 ± 4.8
P1'-1	19.3 ± 4.3	17.8 ± 4.5
P2-m3	24.3 ± 4.3	22.1 ± 4.5
P3-4	17.9 ± 4.8	21.6 ± 4.8
Rupintrivir	23.7 ± 4.7	20.0 ± 5.0

The hydrogen bond (H-bond) formation is one of the essential factors that can determine the binding strength of the interactions between inhibitors and surrounding amino acid residues at the enzyme active site. The intermolecular hydrogen bonds were calculated using the two criteria, i.e., the distance between hydrogen donor (HD) and hydrogen acceptor (HA) ≤ 3.5 Å, and the angle of HD-H...HA $\geq 120^\circ$. The average numbers of H-bond at the last 50 ns from three independent simulations are given in **Table 3**. Again, we found that P2-m3 showed the highest number of hydrogen bonds in CV-A16 and EV-A71 systems (6.5 ± 1.2 and 5.6 ± 1.5), which were more than rupintrivir (4.5 ± 0.9 and 4.7 ± 1.1). These findings suggested that P2-m3 fitted well within the binding pocket of EV-A71 and CV-A16 3Cpro.

Table 3 Number of hydrogen bonds of the focused compounds with CV-A16 and EV-A71 3Cpro calculated from the last 50 ns of the three independent simulations.

	CV-A16	EV-A71
P4-5	4.8 ± 1.1	3.6 ± 1.3
P4-19	4.0 ± 1.2	4.4 ± 1.2
P1'-1	4.0 ± 1.0	5.1 ± 1.1
P2-m3	6.5 ± 1.2	5.6 ± 1.5
P3-4	3.3 ± 1.3	4.8 ± 1.1
Rupintrivir	4.5 ± 0.9	4.7 ± 1.1

By considering the binding pattern in terms of hydrogen bond of P2-m3 in comparison with rupintrivir, the intermolecular H-bonds formed with 3Cpro of EV-A71 and CV-A16 are plotted and illustrated in **Figures 4** and **5**. It can be seen that rupintrivir was stabilized within CV-A16 and EV-A71 3Cpro by forming four H-bonds with the residues in two pocket sites: (i) at P1 site, H161, I162, and K143 residues with O³, N² and N¹ atoms (see atomic labels in **Figure 1B**) and (ii) at P3 site, G164 residue with O⁵ atom. This finding corresponded to the rupintrivir/CV-A16 complex from the X-ray structure [2] and the previous MD study [42]. For the analog P2-m3, the introduction of aminomethyl substitution in meta-position at the P2 site raised the H-bond formation with L127 and K130 in EV-A71 (47.7% and 61.5%) and CV-A16 (40.7% and 77.7%). A medium H-bond with G164 was also detected in CV-A16 3Cpro at the P3 site.

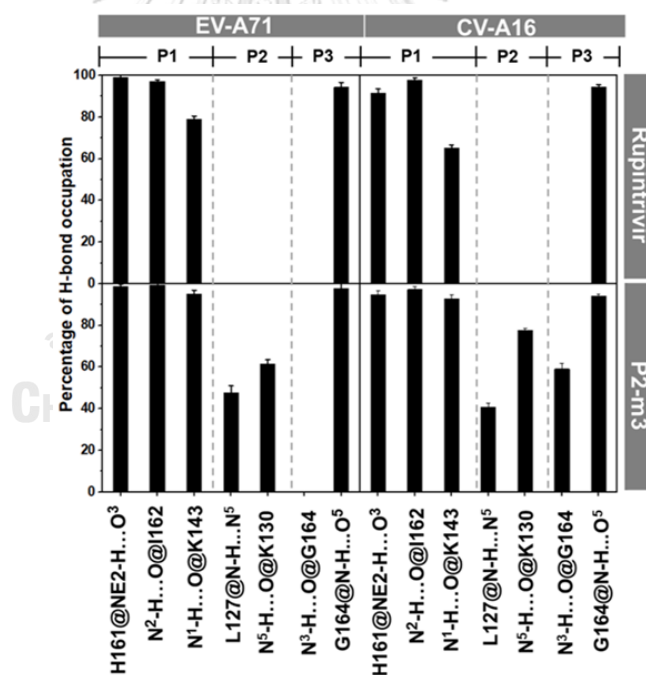


Figure 4 Percentage of intermolecular H-bond occupation with P1, P2, and P3 sites of the rupintrivir and its analog P2-m3 with EV-A71 and CV-A16 3Cpro derived from the last 50 ns simulations, where the representative structures are depicted in Figure 5. Only H-bond occupation >40% is shown in the histogram.

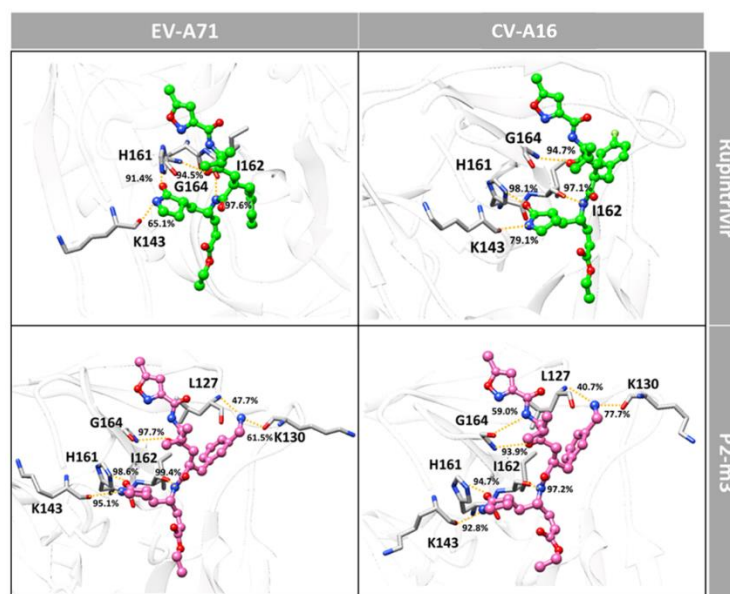


Figure 5 Hydrogen bonding interactions of the rupintrivir and its analog P2-m3 (bond and stick model) with EV-A71 and CV-A16 3Cpro residues (stick model).

3.4. Key Binding Residues

The calculation of per-residue free energy decomposition based on the MM-PBSA method was applied on the 50 frames from the last 50 ns of the three simulations (150 structures in total) to study the critical residues for ligand binding to 3Cpro of CV-A16 and EV-A71. The results are given in **Figures 6 and 7**, where only residues that exhibit the energy stabilization of ≤ -0.5 kcal/mol are labeled and discussed. The key residues binding of CV-A16 3Cpro with rupintrivir were H40, L125, L127, T142, A144, C147, I162, G163, G164, N165, and F170 residues. Likewise, the additional residues K143, G145, Q146, and H161 were in the EV-A71 system. The obtained results were consistent with the previous work [2]. Although the binding pattern of P2-m3 in both targets was likely similar to its template rupintrivir, the residue contribution for P2-m3 binding was more pronounced. Additionally, it was also stabilized by the additional residues F25, N126, S128, and K130 in EV-A71 and F25, S128, K130, K143, Q146, and H161 in CV-A16.

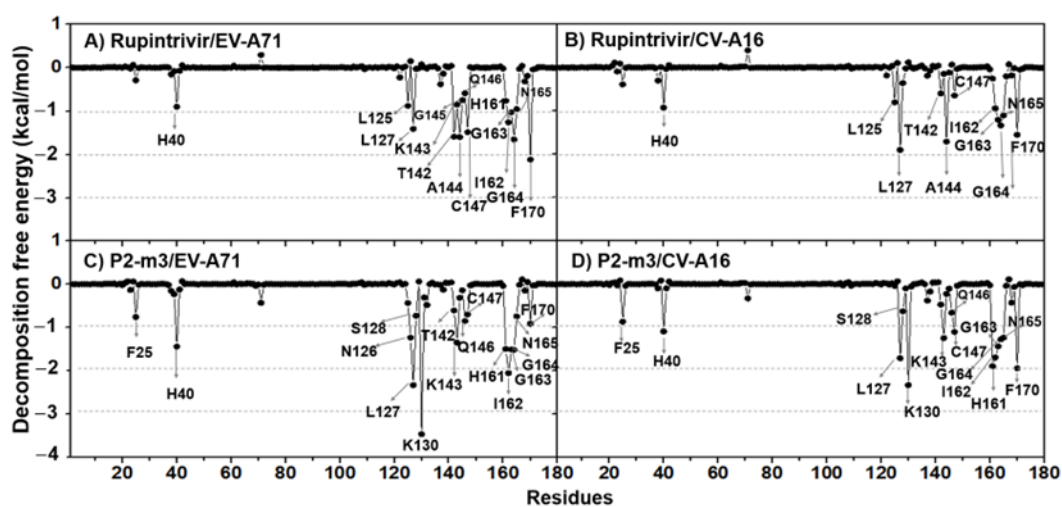


Figure 6 MM-PBSA per-residue decomposition free energy of the rupintrivir and its analog P2-m3 in complex with EV-A71 and CV-A16 3Cpro.

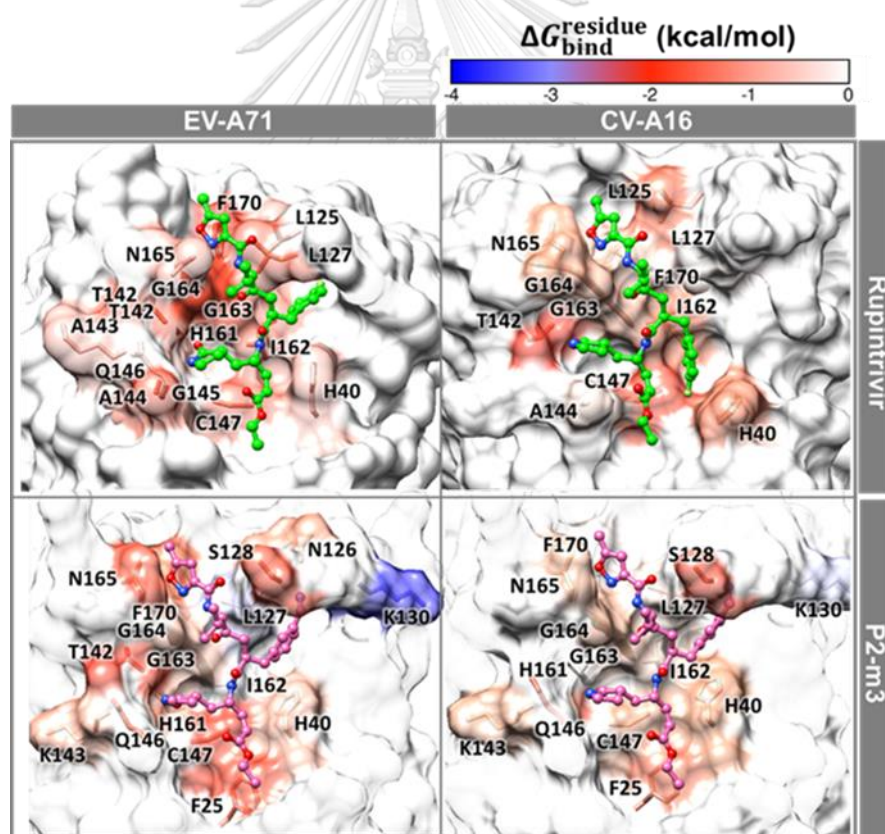


Figure 7 The contributing residues involved in ligand binding are colored according to the per-residue decomposition free energy ($\Delta G_{\text{residue, bind}}$), where the highest to lowest free energies are shaded from white to blue.

3.5. Predicted Binding Affinity of the Potent Rupintrivir Analog

The binding efficiency of the newly designed compound P2-m3 with EV-A71 and CV-A16 3Cpro was estimated by the MM/(GB)PBSA method on the same set of snapshots used in the per-residue free energy decomposition calculation (Table S2). The molecular mechanics energy components in the gas phase (ΔE_{MM}) and binding free energy based on the MM/PBSA method (ΔG_{bind}) results of each system are depicted in Figure 8. The result showed that the P2-m3 had a stronger binding affinity than rupintrivir by ~ 8 and ~ 3 kcal/mol in EV-A71 and CV-A16 (Figure 8B) due to a stronger electrostatic attraction (Figure 8A). Our finding agree with the previous study, which suggested that modification of the P2 residue with a longer side chain can increase the possibility that inhibitor will bind to EV-A71 3Cpro leading to increased inhibitory effect [42]. Changing the fluorobenzyl group at the P2 site of rupintrivir to the aminomethyl-benzyl group in P2-m3 could enhance the ligand-binding affinity in both proteases. Moreover, P2-m3 showed better solubility than rupintrivir from the result of ADMET property (Figure S4).

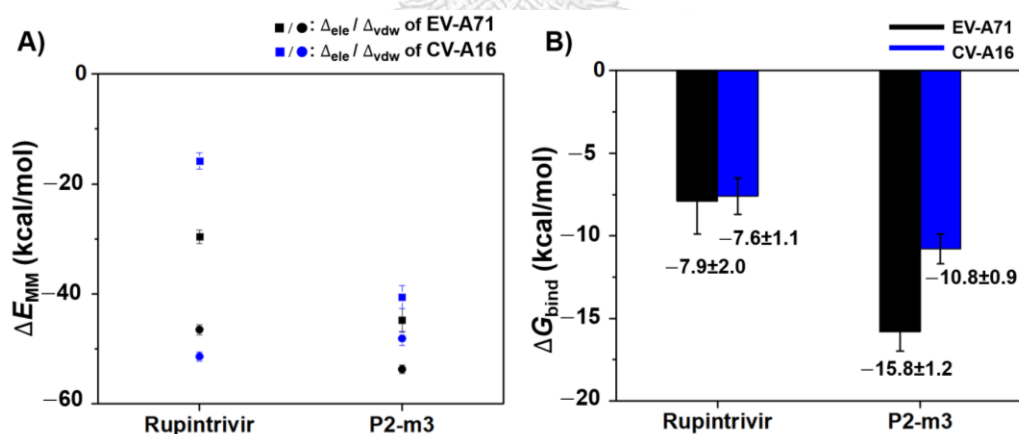


Figure 8 (A) The molecular mechanical energy (ΔE_{MM}) including electrostatic (ΔE_{ele}) and van der Waals (ΔE_{vdw}) interactions and (B) binding free energy (ΔG_{bind}) based on the MM/PBSA method for rupintrivir and P2-m3 binding to EV-A71 and CV-A16 3Cpro.

4. Conclusions

This work provided the newly designed rupintrivir analog P2-m3 with enhanced binding efficiency. By the aminomethyl substitution, this compound showed more hydrogen bonds than rupintrivir with L127 and K130 residue at the P2 site of CV-A16 and EV-A71 3Cpro. A moderate hydrogen bonding with G164 (N³) at P3 was found in CV-A16 3Cpro. Relative to rupintrivir, there was a more significant contribution from the additional key residues for P2-m3 binding, i.e., F25, N126, S128, and K130 in EV-A71 and F25, S128, K130, K143, Q146, and H161 in CV-A16. Altogether, this leads to a better binding affinity of such novel rupintrivir derivative P2-m3 as predicted by the MM-PBSA method. The P2-m3 was suggested to be synthesized and tested for further development as the anti-HFMD agent

Acknowledgment

A.S. thanks the Development and Promotion of Science and Technology Talents Project (DPST) for the scholarship and the 90th Anniversary of Chulalongkorn University Fund (Ratchadaphisaksomphot Endowment Fund, GCUGR1125633083M). S.B. thanks Ratchadaphisaksomphot Endowment Fund of Faculty of Medicine (MF 22/62).

CHAPTER II
MANUSCRIPT II

Discovery of potent compounds against Enterovirus A71 and Coxsackievirus A16
by virtual screening from flavonoid compounds

Amita Sripattarphan¹, Kamonpan Sanachai¹, Siwaporn Boonyasuppayakorn²,
Warinthorn Chavasiri³, Peter Wolschann^{4,5}, Thierry Langer⁴, Phornphimon Maitarad⁶,
Thanyada Rungrotmongkol^{1,7*}

¹ Structural and Computational Biology Research Unit, Department of Biochemistry, Faculty of Science, Chulalongkorn University, Bangkok, Thailand

² Applied Medical Virology Research Unit, Department of Microbiology, Faculty of Medicine, Chulalongkorn University, Bangkok 10330, Thailand

³ Department of Chemistry, Faculty of Science, Chulalongkorn University, Bangkok 10330, Thailand

⁴ Department of Pharmaceutical Chemistry, Faculty of Life Sciences, University of Vienna, Althanstraße 14, A-1090 Vienna, Austria

⁵ Institute of Theoretical Chemistry, University of Vienna, Vienna 1090, Austria

⁶ Research Center of Nano Science and Technology, Shanghai University, Shanghai 200444, PR

⁷ Ph.D. Program in Bioinformatics and Computational Biology, Faculty of Science, Chulalongkorn University, Bangkok 10330, Thailand

* Correspondence: thanyada.r@chula.ac.th, t.rungrotmongkol@gmail.com

Manuscript in preparation for submitting in ACS Omega

Discovery of potent compounds against Enterovirus A71 and Coxsackievirus A16 by virtual screening from flavonoid compounds

Amita Sripattarphan¹, Kamonpan Sanachai¹, Siwaporn Boonyasuppayakorn², Warinthorn Chavasiri³, Peter Wolschann^{4,5}, Thierry Langer⁴, Phornphimon Maitarad⁶, Thanyada Rungrotmongkol^{1,7*}

¹ Structural and Computational Biology Research Unit, Department of Biochemistry, Faculty of Science, Chulalongkorn University, Bangkok, Thailand

² Applied Medical Virology Research Unit, Department of Microbiology, Faculty of Medicine, Chulalongkorn University, Bangkok 10330, Thailand

³ Department of Chemistry, Faculty of Science, Chulalongkorn University, Bangkok 10330, Thailand

⁴ Department of Pharmaceutical Chemistry, Faculty of Life Sciences, University of Vienna, Althanstraße 14, A-1090 Vienna, Austria

⁵ Institute of Theoretical Chemistry, University of Vienna, Vienna 1090, Austria

⁶ Research Center of Nano Science and Technology, Shanghai University, Shanghai 200444, PR

⁷ Ph.D. Program in Bioinformatics and Computational Biology, Faculty of Science, Chulalongkorn University, Bangkok 10330, Thailand

* Correspondence: thanyada.r@chula.ac.th, t.rungrotmongkol@gmail.com

Manuscript in preparation for submitting in ACS Omega

Abstract

Outbreaks of hand, foot, and mouth disease (HFMD) occur around the world caused by the Enterovirus-A71 (EV-A71) and Coxsackievirus-A16 (CV-A16). Up to now, no anti-HFMD drugs are available; therefore, it is interesting to study these viral inhibitors. Rupintrivir, a rhinovirus 3C protease inhibitor, shows an inhibitory activity

for HFMD treatment. In this work, the pharmacophore models of 3C protease of EV-A71 and CV-A16 complexed with the rupintrivir obtained from MD simulations were elucidated. We found both systems showed similar pharmacophore features including hydrogen bond donor, hydrogen bond acceptor and hydrophobic interaction. Subsequently, these pharmacophore models were used as a template for novel inhibitors screening from 39 flavonoid compounds. Among compounds, diosmin, epigallocatechin gallate, EGCG, and RTH-011 showed high binding affinity against EV-A71 and CV-A16. They can interact with important surrounding residues of both proteins such as H40, L127, T142, A144, T145, H161, I162, G163, and G164 with hydrogen bonds. In addition, the effective concentrations against RD cell infection with EV-A71 and CV-A16 of these compounds were also performed. We found that EGCG showed the highest potent efficacy (EC_{50}) at the values of $12.86 \pm 1.30 \mu\text{M}$ and $15.54 \pm 1.50 \mu\text{M}$ for EV-A71 and CV-A16, respectively, while diosmin showed EC_{50} at the values of $21.01 \pm 1.57 \mu\text{M}$ and $30.68 \pm 3.25 \mu\text{M}$ for EV-A71 and CV-A16, respectively. Both compounds were not toxic ($CC_{50} > 250 \mu\text{M}$ and $> 500 \mu\text{M}$ for EGCG and diosmin, respectively) against RD cells. Moreover, the MD simulation analysis revealed that EGCG showed a higher binding affinity than diosmin, supported by significantly lower SIE binding free energies, a higher number of contact atoms, and a higher number of key binding residues similar to rupintrivir. In addition, previous studies reported the inhibitory effect of EGCG with other viruses such as SARS-CoV-2. We suggested that the EGCG compounds effectively inhibit EV-A71 and CV-A16 3C protease.

1. Introduction

Enterovirus A71 (EV-A71) and Coxsackievirus A16 (CV-A16) are single-stranded, viruses-sense RNA viruses belonging to the Enterovirus genus of Picornavirales order. This disease has spread in several Asian-pacific countries, including Australia, Cambodia, China, Japan, Malaysia, Taiwan, Vietnam, and Thailand [30]. The enterovirus can spread quickly through the air by coughing and sneezing by infected patients. Children under the age of 5 years old are sensitive to HFMD infection. The patients have mild fever rashes on the hands, feet, and mouth [7]. Only a small percentage of infected children may rapidly develop severe and even fatal neurological and systemic complications [57]. The positive single-stranded RNA (ssRNA) with a single open reading frame (ORF) encoding a viral polyprotein precursor is present in both viruses. The activity of 3C proteases results in the production of a viral polyprotein and further cleaved into the four structural proteins (2A, 2B, 2C, 3A, 3B, 3C, and 3D) by the activity of 3C proteases (3Cpro) [2]. The 3Cpro (**Figure 9**) is a cysteine protease that favorably splits the peptide bond between glutamine (Q) and glycine (G) of viral protein through a reaction involved in catalytic triad residues (H40, E71, and C147) [9]. The 3C protease is a prime target for the development of anti-HFMD drugs due to its critical function in the life cycles of EV-A71 and CV-A16. The antiviral drug candidate rupintrivir (AG7088) is a potent peptidomimetic inhibitor of human rhinovirus (HRV) 3C protease. Additionally, rupintrivir exhibits a broad-spectrum antibiotic activity against other members of the family Picornaviridae [12] such as CVB2, CVB5, EV6, and EV9 [33, 34, 36, 58]. Interestingly, its activity significantly decreases in EV-A71 approximately ~100-fold compared to HRV [59]. In previously reported, the rupintrivir can inhibited the 3C pro of EV-A71 on enzyme-based assay (IC_{50} of 1.65 μ M) [2] and Vero cell growth inhibition (EC_{50} of 0.78 μ M) [8] has been reported. However, more specific and potent CV-A16 and EV-A71 3Cpro inhibitors are imperatively necessary.

Flavonoids are naturally polyphenolic compounds widely distributed in plants and are effective for various biological functions [16]. They have become compounds of interest for natural drug discovery research. Flavonoids have several pharmacological properties including antioxidant, anti-inflammatory, anticancer, and antiviral [17]. A previous study reported that quercetin was shown to inactivate the NS5 protease of the hepatitis C virus (HCV) [60]. Moreover, a few flavonoid compounds including myricetin, astragaloside, rutin, epigallocatechin gallate, epicatechin gallate, gallic acid, and luteolin inhibited the ZIKA NS2B-NS3pro activities more than 40% [61].

Nowadays, several computational techniques have become the most effective methods in drug discovery and development. A pharmacophore-based screening approach is one of the most practical tools for the fast and accurate virtual screening of databases with millions of compounds that match the similarity of the three-dimensional (3D) interaction pattern or pharmacophore model of drug-like compounds with known ligands in the complexes [2, 16, 17, 60]. A previous study reported the discovery of novel inhibitors of HCV polymerase from the chemical library from Asinex Ltd (233,554 compounds) by pharmacophore-based virtual screening which used HCV-796 as a reference inhibitor. It showed hydrogen donor, hydrogen acceptor, and lipophilic interaction features. They obtained 18 hits and tested inhibitory efficiency for HCV polymerase in vitro. The compound 1 and 2 showed 54% and 48% inhibitions at 20 μ M, respectively [62]. This study aimed to find new potential compounds against 3C protease of EV-A71 and CV-A16 from flavonoids by using pharmacophore-based virtual screening (**Figure 10**). Subsequently, molecular docking was used to study the binding interactions at the atomic level of potent compounds with 3C protease of EV-A71 and CV-A16. Finally, the potent compounds' cytotoxicity and antiviral efficacy against EV-A71 and CV-A16 infection in human rhabdomyosarcoma (RD) cells were also performed.

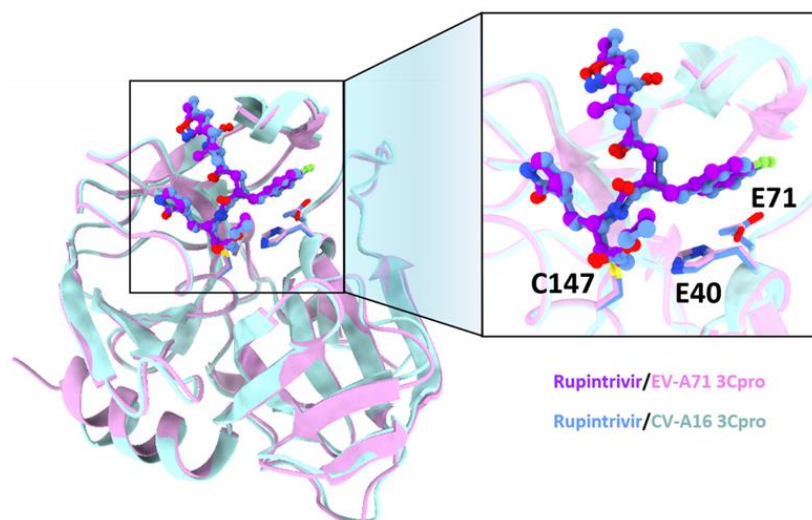


Figure 9 The superimposition structure of EV-A71 (PDB ID: 3R0F) and CV-A16 (PDB ID: 3SJI) in complex with rupintrivir (ball and stick model).

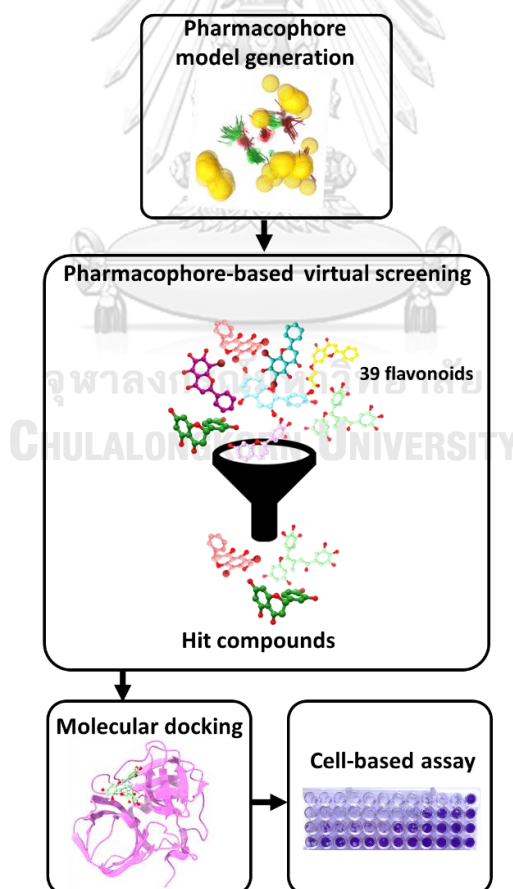


Figure 10 The workflow of this work for searching a newly potent compound against EV-A71 and CV-A16.

2. Material and Methods

The overview of this work for searching for a newly potent compound against EV-A71 and CV-A16 is summarized in **Figure.10**. Initially, we generated pharmacophore features of rupintrivir/EV-A71 and CV-A16 complexes and used them as the template for searching the potent compounds among 39 flavonoids. Then, the potent compounds were studied the binding mechanism using molecular docking. Finally, cell based-assay was performed to evaluate the antiviral activity of potent compounds

2.1. Pharmacophore modeling

2.1.1 Pharmacophore modeling

A total of 7500 frames from a trajectory over the last 50 ns simulation of CV-A16 and EV-A71 3Cpro-rupintrivir complexes were used to create pharmacophore models at the binding site using the LigandScout 4.4.2 program in the KNIME analysis platform [63, 64]. The MD trajectories were the eliminated waters and ions. The PDB reader and DCD trajectory reader nodes were created for loading information on complex structures and trajectories. We generated the pharmacophore features of rupintrivir/EV-A71 and CV-A16 3Cpro via the "Pharmacophore creator" node in the KNIME program with default parameters. The pharmacophore clustering node was created by the unique pharmacophore models by chemical features clustering. Then, these unique pharmacophore models were clustered to a representative pharmacophore model (RPMs). These RPMs in each system were reached from the "Pharmacophore writer" node. All RPMs were used as a template for novel inhibitors screening.

2.1.2. Virtual screening

The 39 flavonoid compounds in the library were screened for each RPM by using "get best matching conformation" in retrieval mode, and checked exclusion volume based on the pharmacophore-fit scoring function [65]. For the potent compounds, they were chosen because they had similar features that match the pharmacophore features of the reference drug. The hit-lists were created in SDF

file format and visualized by the Ligand Scout 4.2 program. The hit compounds with a higher pharmacophore-fit score than rupintrivir were chosen to study in the following steps.

2.1.3. Model validation

The accuracy of screening results was validated by the receiver operating characteristic curve and the area under this curve (ROC-AUC). The area under the ROC curve (AUC) was used for method validation [66]. For comparison, Decoys (inactive compounds) were designed to mimic the active molecule structure. Decoys were obtained from the Zinc database [12]. The ROC values were gathered from the individual RPM screening with active and decoy datasets. Then, the values of screening results were plotted and interpreted in terms of sensitivity (true positive rate, TPR) and specificity (false positive rate, FPR). Sensitivity and specificity measurements were calculated using the following equations.

$$\text{Sensitivity} = \frac{\text{Selected active ligands}}{\text{All selected ligands}} \quad (1)$$

$$\text{Specificity} = \frac{\text{Discarded inactive ligands}}{\text{All inactive ligands}} \quad (2)$$

2.1.4. Molecular Docking

The crystal structures of rupintrivir with 3Cpro of EV-A71 (PDB ID: 3R0F) and CV-A16 (PDB ID: 3SJI) were downloaded from the Protein Data Bank. The 3D structure of the rupintrivir was obtained from the ZINC database, whilst the potent compounds were generated and optimized HF/6-31G(d) method achieved in the Gaussian09 software [46]. The potent ligands were predicted the protonation states (**Fig. S1**) at physiological pH 7.4 by MarvinSketch 21.20 [67, 68]. For validation of the system, the reference ligand (rupintrivir) was redocking into a center in the active site of both proteins by using GOLD programs, which are based on a genetic algorithm (GA). The 15 Å for the sphere of compound docking and GOLD scoring function were set for both EV-A71 and CV-A16 systems. All systems were performed as 100 docking

poses. The UCSF ChimeraX ver.1.3 and Accelrys Discovery Studio 2.5 (Accelrys Inc.) were utilized to visualize the binding between proteins and compounds.

2.2. Antiviral cell-based study

2.2.1. Cells and viruses

Human rhabdomyosarcoma cells (RD) were cultured in Dulbecco's modified Eagle's medium (DMEM) (Gibco, Langley, USA) supplemented with 10% fetal bovine serum acid (Sigma Aldrich, St. Louis, USA), 100 I.U./ml and 100 µg/ml streptomycin (Bio Basic Canada, Ontario, Canada), and 10 mM HEPES (4-(2-hydroxyethyl)-1-piperazineethanesulfonic acid) (Sigma Aldrich, St. Louis, USA) at 37 °C under 5% CO₂. Eterovirus-A71 (EV-A71) and Coxsackievirus-A16 obtained from the Asst.Prof.Siwaporn Boonyasuppayakorn, Faculty of Medicine, Chulalongkorn University, Thailand. Department of Medical Science was propagated in RD cell line with DMEM supplemented with 1% fetal bovine serum at 37 °C under 5% CO₂.

2.2.2. Cytotoxicity study

RD cells were seeded at 5×10^4 cells per well of a 96-well plate and incubated overnight. Compounds were prepared to 6–10 different concentrations in filter-sterilized dimethyl sulfoxide (Merck, Darmstadt, Germany) before addition to the cells. The plates were incubated for 48 h before the MTS reagent (Promega, Madison, WI, USA) was added to cells according to the manufacturer's protocol and incubated for 4 h before analysis by spectrophotometry at 560nm. Each compound was tested in triplicate. Cytotoxic concentrations (CC₅₀) were calculated using non-linear regression analysis and the results were reported as means and standard deviations of three independent experiments.

2.2.3. Antiviral efficacy of selected compounds

RD cells were seeded at 2.5×10^5 cells per well of a 24-well plate in a growth medium and incubated overnight at 37 °C under 5% CO₂. Cells were infected with EV-A71 and CV-A16 at the multiplicity of infection (MOI) of 0.1 for 1 h with gentle rocking every 15 min. Cells were washed with PBS and incubated with DMEM supplemented with 1% fetal bovine serum, 100 I.U./mL penicillin, and 100 µg/mL streptomycin. The selected compounds from pharmacophore modeling techniques

were prepared in dimethyl sulfoxide (DMSO) and added to the virus-infected cells during and after infection. The cells were incubated for 72 h, unless otherwise indicated, at 37 °C under 5% CO₂. Supernatants were collected and the viral infectivity was analyzed by 96-well plaque titration. After plaques became visually apparent by microscopy, cells were fixed and stained with 10% formaldehyde (Carlo Erba, Milano, Italy), 5% isopropanol (Merck, Darmstadt, Germany), and 1% crystal violet (Merck, Darmstadt, Germany) for 1 h. The number of plaques forming units (p.f.u.) per ml was determined manually [69]. Data were plotted, and the EC₅₀ values were calculated by nonlinear regression analysis. The results were reported as means and standard deviations of three independent experiments. The selectivity index was calculated from the ratio of CC₅₀ and EC₅₀.

2.3. Molecular dynamic simulation

The potent ligands from the antiviral cell-based study were simulated under periodic boundary conditions with an NPT ensemble. The short-range cutoff for nonbonded interactions is set as 10 Å, and the particle mesh Ewald summation method [70] was used to treat the electrostatic interactions. The SHAKE algorithm is used to constrain all covalent bonds involving hydrogen atoms. A simulation time step of 2 fs was used along with the MD simulation. The Langevin thermostat [42] with a collision frequency of 2 ps⁻¹ was employed for temperature control, while the Berendsen [14] barostat with a pressure-relaxation time of 1 ps was used to maintain the standard pressure of the system. The simulated models are then heated up to 310 K for 100 ps and are continuously held at this temperature for another 500 ns or until the simulations have reached equilibrium [55], which mean the complexes were stable during the simulations. Each complex was simulated three independent MD runs by the difference velocity. Finally, the CPP-TRAJ [54] was used to calculate the root-mean-square deviation (RMSD), the number of contact atoms, intermolecular hydrogen bonding between ligand/3Cpro, binding free energy, decomposition binding energy, and motion of protein by PCA analysis.

3. Results and Discussion

3.1 Pharmacophore models and virtual screening

Pharmacophores were defined as molecular electronic features necessary for the molecular recognition of potent compounds with a specific biological target [71]. In this study, the pharmacophore features of rupintrivir with EV-A71 and CV-A16 were generated from 7500 MD snapshots in previous work. According to **Figure 11.**, all RPMs are mainly described by the hydrophobic properties (yellow sphere), hydrogen bond donor (HBD; green arrow) and hydrogen bond acceptor (HBA; red arrow). All pharmacophore models were aligned and clustered. Subsequently, the 100 unique pharmacophore models were obtained for a representative pharmacophore models (RPMs). The generated pharmacophore features of rupintrivir with EV-A71 consist of hydrophobic interactions with L127, T132, A144, and F170, three HBDs with T142, I162, and G164, and three HBAs with S128, G145 and C147, and G164. For the CV-A16 complex, most of the pharmacophore features were similar to the EV-A71 complex. We found hydrophobic interactions with F25, A144, and F170, three HBDs with T142, C147, and G164, and three HBA with G145, C147, and G164. The interaction with the percentage greater than 50% were labeled and considered to be the main interaction for binding. Moreover, We noticed that most of interaction residue in both protein with rupintrivir were consistent with the key binding residues of previous study [72]. The RPMs of each complex were used as the template for searching the potent compounds against EV-A71 and CV-A16 using the 39 flavonoids database. We found 4 and 6 hit compounds (including rupintrivir) for EV-A71 and CV-A16, respectively (**Table 4**). Based on the pharmacophore fit score, we were only focused on compounds with higher scores than the rupintrivir in EV-A71 (score of 46.8) and CV-A16 complexes (score of 46.9), including diosmin, EGCG, and RTH-011. Therefore, these three compounds were selected to elucidate in the next step.

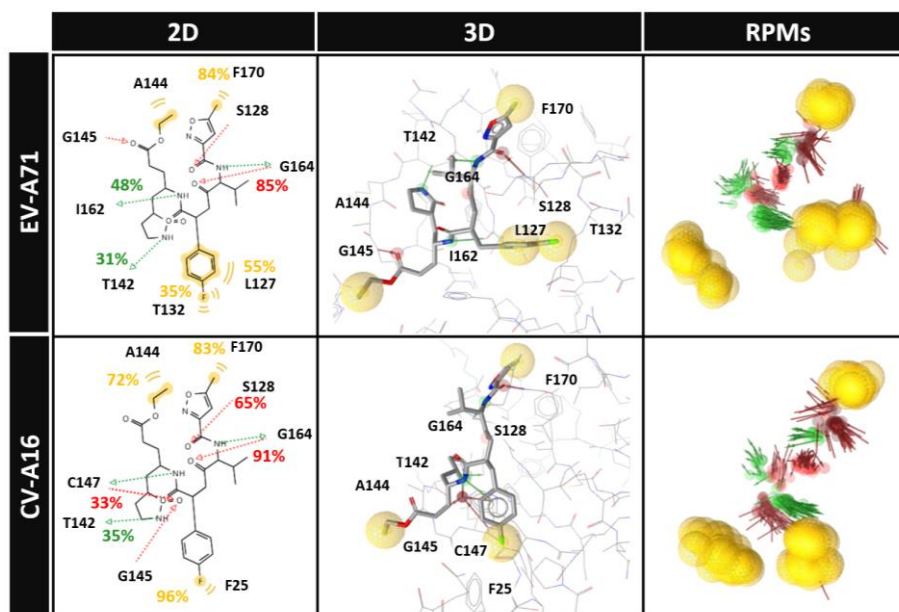


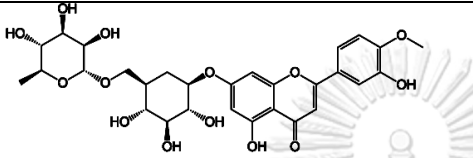
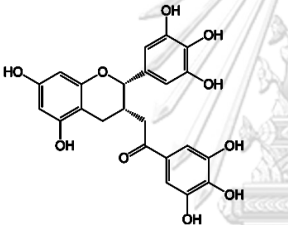
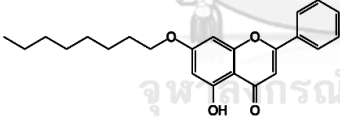
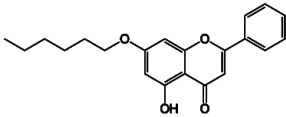
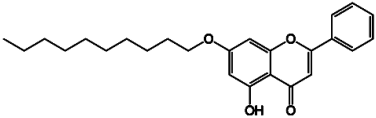
Figure 11 The 2D and 3D pharmacophore models of the rupintrivir/EV-A71 and CV-A16 3C protease complexes and the interacting residues extracted from the first snapshot of the last 50 ns MD trajectories. The pharmacophore features are represented as green arrows (HBD), red arrows (HBA), and yellow spheres (hydrophobic property). The interaction with the percentage greater than 30% were labeled and considered to be the main interaction for binding.

3.2 Virtual Screening Validation

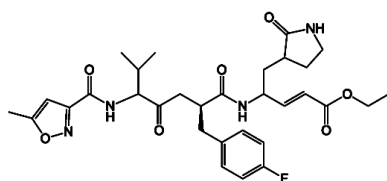
The receiver operating characteristic curve and the area under this curve (ROC-AUC) were conducted to validate screening accuracy. The performance of screening and the ability to identify between 144 decoys and 4 active compounds (including reference ligand) for the EV-A71 system and 216 decoys and 6 active compounds was achieved by ROC plot. The area under the curve (AUC) represents the quality of the ROC plot, which should be >0.50 . It means the results from this method are reliable [73]. The results showed that the AUC values are 1.00 (1%), 1.00 (5%), 1.00 (10%), and 0.72 (100%) for EV-A71 (**Fig.12A**). CV-A16 system showed 1.00 (1%), 1.00 (5%), 1.00 (10%), and 0.82 (100%) (**Fig.12B**). Our model could distinguish true actives from decoy compounds [74]. Therefore, the obtained hit compounds

from pharmacophore-based screening are acceptable for further antiviral drug development.

Table 4 List of hit compounds, pharmacophore fit score and fitness score against EV-A71 and CV-A16

Compound	Structure	Pharmacophore fit score		Fitness score	
		EV-A71	CV-A16	EV-A71	CV-A16
Diosmin		47.7	47.9	69.3	64.0
EGCG		47.6	47.7	60.6	60.5
RTH-011		47.0	47.4	56.2	53.9
RTH-010		-	45.5	-	-
RTH-012		-	45.5	-	-

Rupintrivir
(reference)



46.8 46.9 84.9 65.0

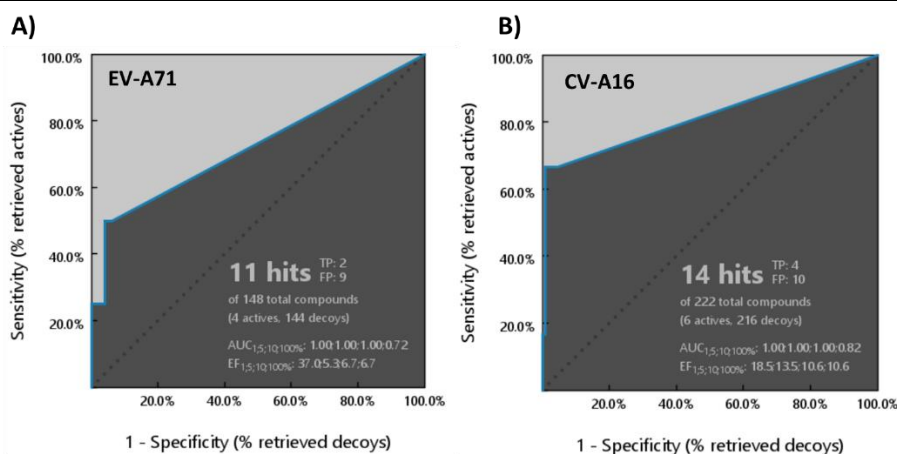


Figure 12 Receiver operating characteristic (ROC) plot of pharmacophore model applied to EV-A71 and CV-A16 3C protease. The area under the curve (AUC) is given for 1, 5, 10, and 100% of the database.

3.3 Molecular docking of potent compounds

To investigate the binding mechanism of the potent compounds (Diosmin, EGCG, and RTH-011) towards EV-A71 and CV-A16 3Cprotease compared to the reference drug (rupintrivir), molecular docking was performed by using GOLD. The potent compounds and rupintrivir were docked into the active site of EV-A71 and CV-A16 3Cpro (Figure 13). The fitness score is given in Table 4. We found that the fitness score of rupintrivir was higher than all potent compounds in both complexes. The binding interaction between ligand-protein is shown in Figure 14 and Figure S2. Rupintrivir could interact with surrounding residues of EV-A71 in the substrate binding sites via four H-bonds (R39, T142, G164), four pi-alkyl (Y122, L125, L127, F170), one pi-sigma (L125), and one halogen bond (E71). While CV-A16 system, rupintrivir formed five H-bonds (S128, G145, Q146, C147, and G164), four pi-alkyl (L125, L127, and K130), one pi-sulfur (R39), and one halogen bond (E71). The obtained surrounding residues of rupintrivir were consistent with the critical binding residues of previous

work, which are residues L125, L127, T142, A144, C147, I162, G163, N165, and F170 for rupintrivir/EV-A71 [2, 42]. For EV-A71, all potent compounds can interact with the key binding residues similar to rupintrivir/EV-A71 but showed no pi-sigma interaction with L125 residue. Moreover, we noticed that EGCG was the only compound that found pi-pi stacked with H40 residue. Interestingly among compounds and rupintrivir, diosmin showed the highest number of H-bonds (eight H-bonds with Q22, T142, K143, C147, H161, and I162), while EGCG revealed the highest number of pi-alkyl with five residues, H40, L127, A144, C147, and I162). Moreover, diosmin was the only compound that found pi-sulfate interaction with residue C147.

For CV-A16, the obtained results are pretty similar to EV-A71. Diosmin also had the highest number of H-bonds similar to diosmin/EV-A71 (seven H-bonds with R39, Q42, L127, S128, T142, H161, and I162). Whereas, EGCG showed the highest number of pi-alkyl with four residues, H40, L127, A144, and C147). All potent compounds can interact with the critical binding residues (H40 and C147) but had no pi-cation at R39 of rupintrivir/CV-A16. We only found pi-sulfur with C147 in the diosmin complex and pi-pi stacked with H40 of EGCG and N165 of diosmin. Moreover, we found van der Waals (vdW) interaction in all systems, but rupintrivir/EV-A71 showed the highest number of vdW interaction than other systems. RTH-011 showed low interacting residues with both protein complexes compared with other ligands. They are related to the RTH-011 fitness score, which is the lowest value for both protein complexes. These findings suggested that only diosmin and EGCG fitted well within the binding pocket of EV-A71 and CV-A16 3Cpro.

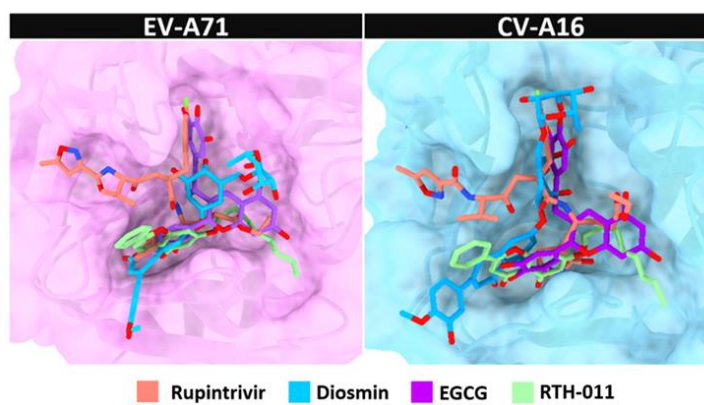


Figure 13 The potent compounds were docked into the active site of EV-A71 and CV-A16 3Cpro which has rupintrivir as a reference drug.



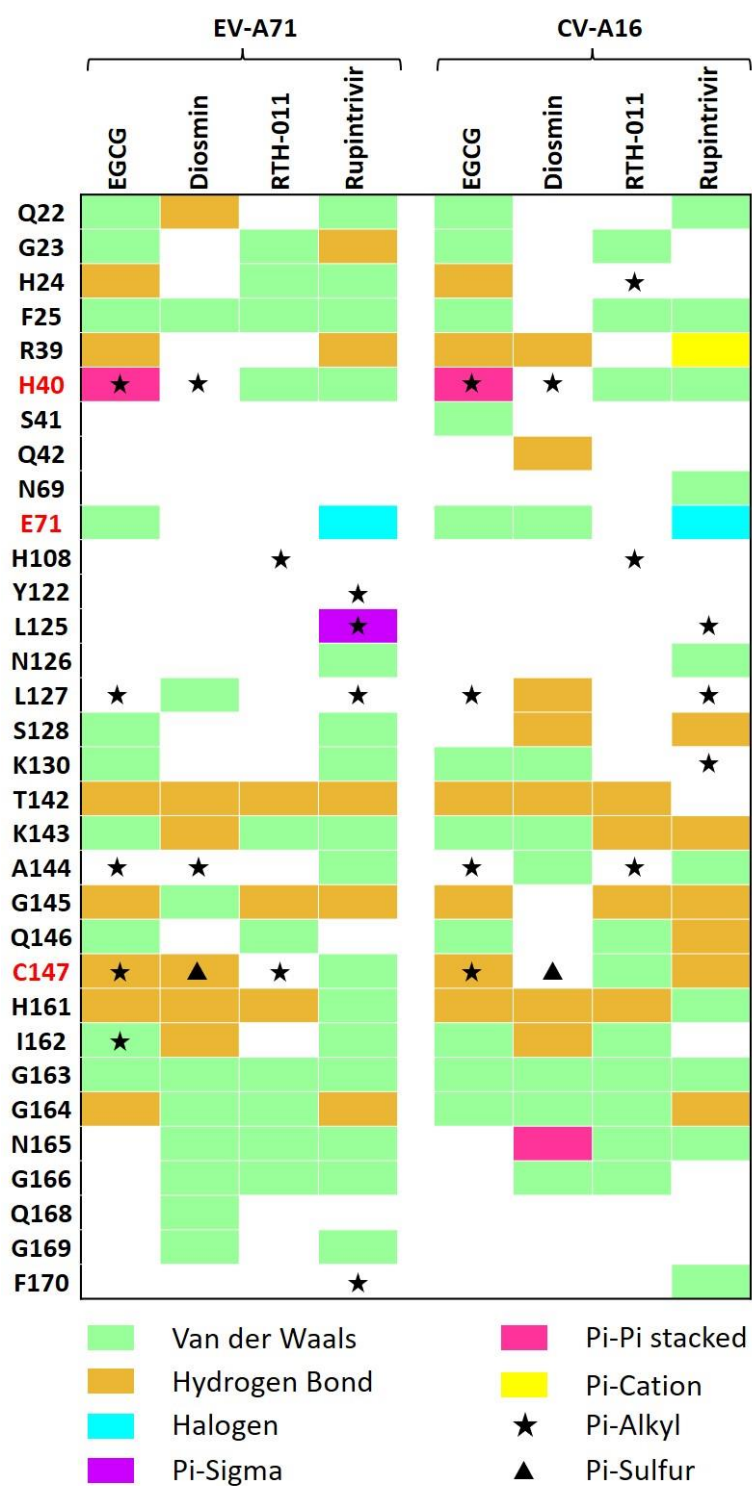


Figure 14 The 2D interactions of potent compounds and rupintrivir in EV-A71 and CV-A16 3Cpro complexes. The residues with black label were substrate binding residues while the residues with red label were critical binding residues.

3.4 Cytotoxicity and Inhibitory effect of the potent compound

Before applying the potent compounds into the antiviral assay, the cellular toxicity of Human rhabdomyosarcoma (RD) cells was assessed to evaluate the 50% cytotoxic concentration (CC_{50}) using the MTS assay. Note that the diosmin and EGCG compounds were completely dissolved in DMSO, whereas the RTH-011 was insoluble. The obtained results (**Figure 15.**) revealed that both compounds were not toxic against cells ($CC_{50} > 250 \mu\text{M}$ and $> 500 \mu\text{M}$ for EGCG and diosmin, respectively). In agreement with the previous study reported that flavonoid compounds, chrysin and quercetin have no detectable cytotoxicity to RD cells at the concentration of $200 \mu\text{M}$. Subsequently, the RD cell was infected by EV-A71 and CV-A16 to investigate the inhibitory activity of diosmin and EGCG. A plaque assay was performed to evaluate the half-maximal effective concentration (EC_{50}) values as shown in **Figure 16.** For EV-A71, the EC_{50} of diosmin and EGCG were $21.02 \pm 1.57 \mu\text{M}$ and $12.86 \pm 1.30 \mu\text{M}$, respectively. For CV-A16, the EC_{50} of diosmin and EGCG were $30.68 \pm 3.25 \mu\text{M}$ and $15.54 \pm 1.50 \mu\text{M}$, respectively. The results showed that both compounds could reduce the viral titer of EV-A71 and CV-A16. Moreover, a previous study reported that other flavonoid compounds such as chrysin, apigenin, hydroxyflavone (HF), and quercetin can block EV-A71 proliferation with an EC_{50} of $15.89 \mu\text{M}$, $10.3 \mu\text{M}$, $23.45 \mu\text{M}$, and $12.1 \mu\text{M}$ [75-78]. Therefore, EC_{50} of diosmin and EGCG are consistent with other flavonoid compounds mentioned above with similar values. Additionally, there were many reports about the antiviral activity of EGCG, which can inhibit influenza A (EC_{50} of $22\text{--}28 \mu\text{M}$), porcine epidemic diarrhea virus (EC_{50} of $12.39 \mu\text{M}$), and zika virus (EC_{50} of $21.4 \mu\text{M}$) [79-81]. Moreover, we found that both of compounds had similar selective index. (Table S1). We suggest that EGCG and diosmin had potentially antiviral activity against EV-A71 and CV-A16 infection. The result showed that the EC_{50} of EGCG and diosmin in EV-A71 was lower than CV-A16. Therefore, Both compounds with EV-A71 were selected to study in the next step.

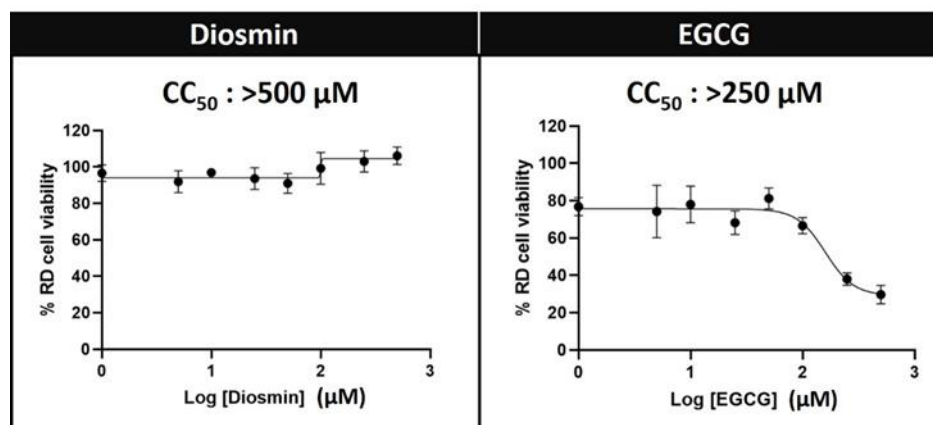


Figure 15 Cytotoxicity of diosmin and EGCG against RD cells using MTS assay. The compounds were dissolved in DMSO and diluted into eight concentrations (1, 5, 10, 25, 50, 100, 250, and 500 μM)

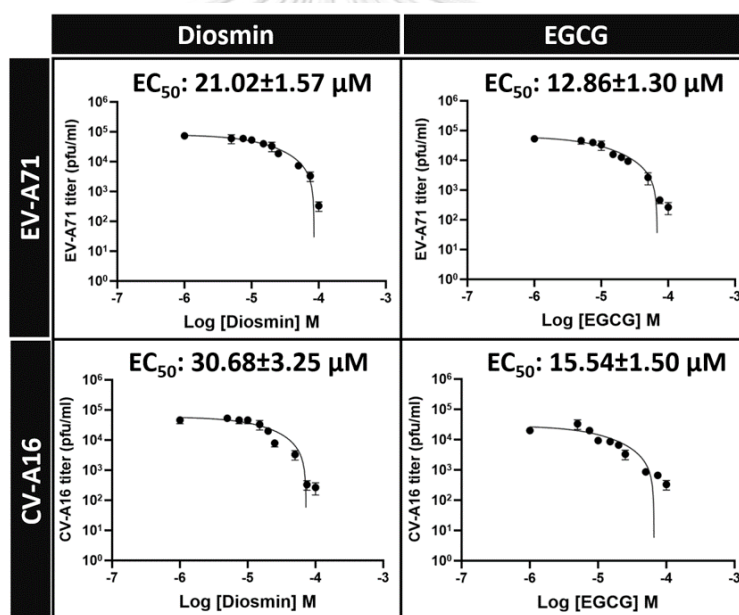


Figure 16 Inhibitory activity of diosmin and EGCG toward RD cell infection by EV-A71 and CV-A16.

3.5 Mechanism of potent compounds binding

To investigate how EGCG and diosmin showed potential EV-A71 3Cpro inhibition at the molecular level, the binding of each potent compound at the active site was investigated by 500-ns MD simulation. The stability of the EGCG and diosmin with EV-A71 complexes were characterized using the root mean square displacement

(RMSD) calculation plotted along the simulation time (500 ns), and the obtained results are illustrated in **Figure 17A**. The RMSD values of both systems were about 1.0–2.0 Å from the beginning of the simulation until the end. It means the systems were likely stable along with the simulations in the active site and reached the equilibrium state. In the study, the last 50 ns of simulations were examined for the further analysis in terms of the number of H-bond (#H-bonds), the number of contact atoms (#contact atom) within the 3.5 Å sphere of EGCG, and diosmin in the active site, binding free energy and motion of protein by PCA analysis.

According to the results, EGCG and diosmin showed similar #H-bonds (4.4 ± 1.2 and 4.5 ± 1.3 , respectively) in **Figure 17B**. In contrast, EGCG showed a higher #contact atom than diosmin (26.3 ± 5.8 and 17.4 ± 4.7 , respectively) in **Figure 17C**. In addition, we found diosmin was stabilized within EV-A71 3Cpro by forming H-bonds with the residues Q22, H24, H40, and T142, while EGCG formed H-bonds with the residues Q22, E71, and H161 (**Figure 17D**). These findings suggested that EGCG fitted well within the binding pocket of EV-A71 3Cpro.

The decomposition energy calculation was performed based on the MM-PBSA method to characterize the critical residues involved in potent compound binding. The $\Delta G_{bind}^{residue}$ are plotted in **Figure 18**. shows and discusses only residues with an energy stabilization of less than 0.5 kcal/mol. From the result, diosmin showed ten residues, including Q22, G23, H24, F25, H40, C147, G163, G164, N165, and G166. For EGCG, it showed 13 residues, including Q22, H40, E71, L127, T142, K143, A144, Q146, C147, H161, I162, G163, and G164. It indicated that EGCG can interact with the residues in the pockets more effectively than diosmin. We noticed that some key binding of both compounds were consistent with rupintrivir's key binding residues of the previous work [72]. Diosmin showed five residues (H40, C147, G163, G164, and N165) which were similar to the key binding residues of rupintrivir, while EGCG showed eleven residues (H40, L127, T142, K143, A144, Q146, C147, H161, I162, G163, and G164). We observed that both compounds could bind to the catalytic residues (H40, E71, and C147) effectively [9]. The EGCG had lower binding free energy

compare to the diosmin. Moreover, we found that Q22 and E71 with low binding free energy were consistent with strong H-bond formation in **Figure 17D**. These findings suggested that EGCG had binding affinity better than diosmin and was similar to rupintrivir.

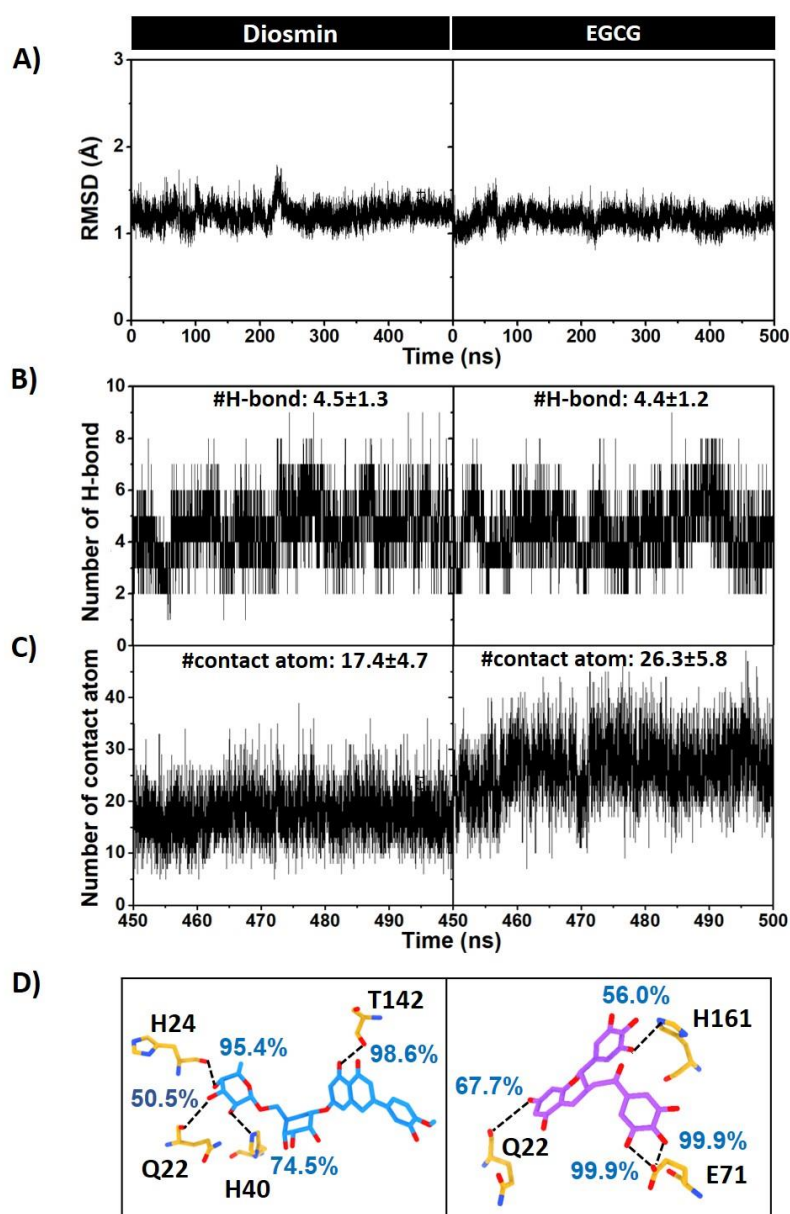


Figure 17 A) All-atom RMSD (500ns MD simulation), B) number of contacts atom, and number of H-bonds of diosmin and EGCG in complex with EV-A71 3Cpro plotted along the last 50 ns MD simulation. The percentages of hydrogen bond occupation are shown in D).

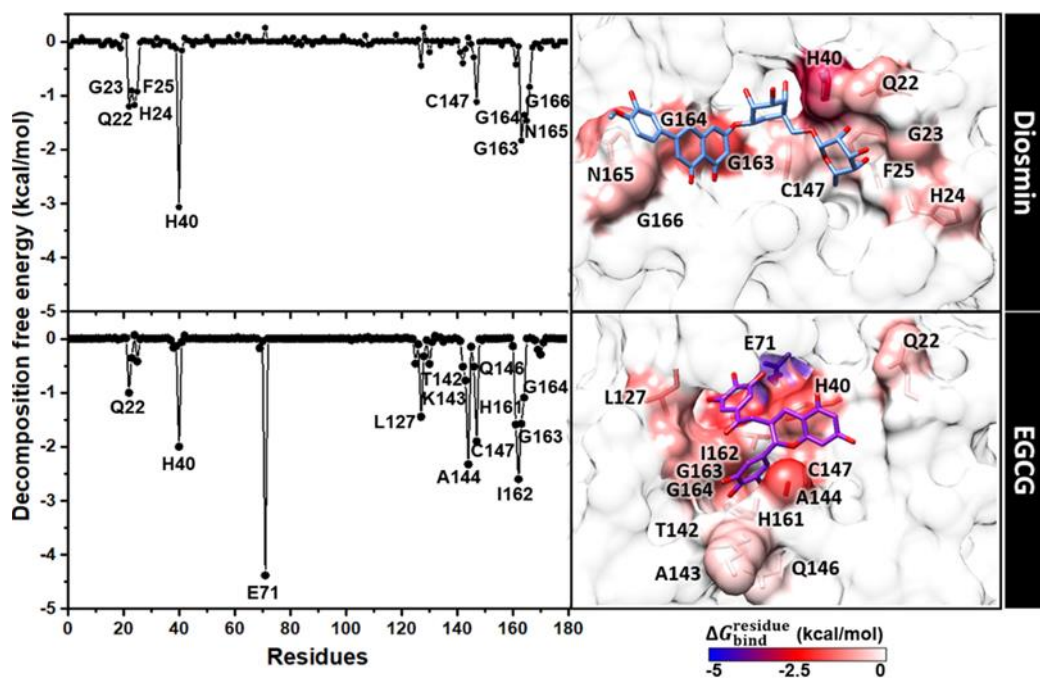


Figure 18 MM-PBSA per-residue decomposition free energy of the diosmin and EGCG in complex with EV-A71 3Cpro. The contributing residues involved in ligand binding are colored according to the per-residue decomposition free energy ($\Delta G_{\text{residue, bind}}$), where the highest to lowest free energies are shaded from blue to yellow.

Table 5 The energy components (kcal/mol) of potent compounds/3Cpro calculated with the SIE method

Energy components	Diosmin	EGCG
E_{vdw}	-40.67±3.24	-45.75±4.14
E_{ele}	-45.12±5.29	-24.86±3.87
ΔG_{RF}	49.58±4.36	20.89±2.52
ΔG_{cavity}	-6.96±0.51	-7.51±0.30
ΔG_{bind}	-7.41±0.42	-8.89±0.41

In addition, these findings were supported by the binding free energy of each complex derived from SIE method calculation. The result (**Table 5**) showed that the EGCG had a stronger binding affinity than diosmin by ~1.5 kcal/mol. Since the majority of residues that interact with EGCG are non-polar, the primary interaction is with van der Waals (vdW).

To understand the dominant motions of EV-A71 3Cpro during compound binding in the active site, a principal component analysis (PCA) is a helpful method for inspection the motion of protein along MD trajectories. The last 50 ns MD trajectories of apo and holo proteins were used for PCA. The PCA scree plot of the first 10 PC modes is plotted in **Figure 19A**. The covariance matrix of atomic fluctuation data was diagonalized to build a two-dimensional (2D) projection on the PC1 and PC2 in **Figure 19B**. The result showed that EGCG bound the EV-A71 3Cpro could raise the percentage of variances of PC1 from 11.4% to 14.2%. Moreover, we found that the conformational distributions of the holo form of both complexes were greatly different from those of the apo form. The holo forms showed a lower distribution in 2D projection on the first two PCs. In addition, the porcupine plot of both systems from the first principle component PC1 is shown in **Figure 20**. The head of the arrows serve as the direction of active site residue motions and the length of the arrow represented the amplitude of movement. We noticed that EGCG and diosmin could stabilize the complexes with turning structural from open conformation to closed conformation. The residues in the active site with both compounds, they moved towards the ligand binding in the holo form with close conformation. This finding suggested that EGCG and diosmin could effectively stabilize the EV-A71 3Cpro.

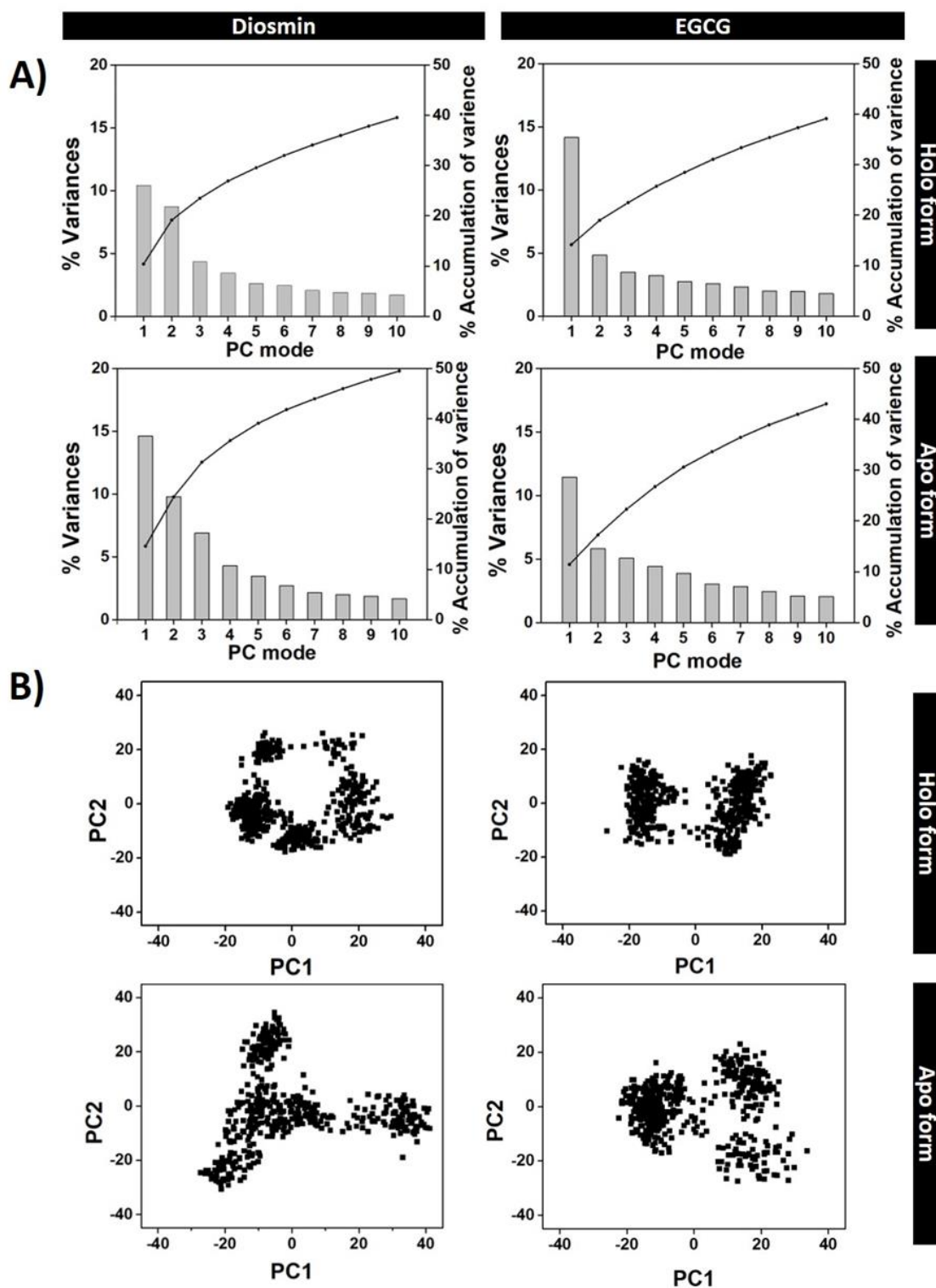


Figure 19 A) PCA scree plot of PC modes and B) the 2D projection of first two PC modes, derived from MD trajectories of the EV-A71 3C protease apo form and holo form with diosmin and EGCG.

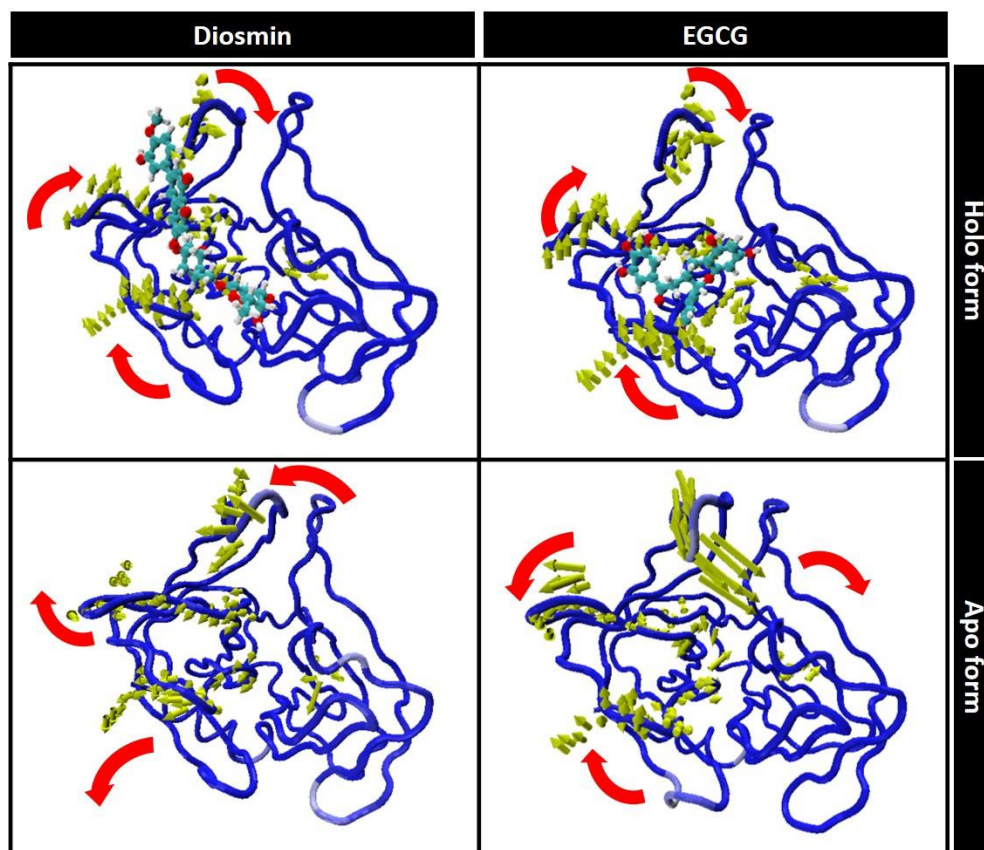


Figure 20 The porcupine plots corresponding to PC1 obtained from PCA analysis of apo form and holo form with diosmin and EGCG/EV-A71 3Cpro. The head of the arrow (yellow) represents the direction of motion, while its length represents the amplitude of the protein motion.

จุฬาลงกรณ์มหาวิทยาลัย
CHULALONGKORN UNIVERSITY

4. Conclusions

This work provided the newly potent compound against EV-A71 and CV-A16 derived from flavonoid compounds using pharmacophore-based screening. The EGCG and diosmin were potentially EV-A71 and CV-A16 inhibitions. For molecular binding, the EGCG stabilized within the binding pocket of EV-A71 3Cpro with H24, R39, H40, L127, T142, A144, G145, C147, H161, and G164 residues, while diosmin interacted with Q22, H40, T142, K143, A144, C147, H161, I162 G163, G164 residues were obtained. For CV-A16 3Cpro, EGCG can interact with similar residues to EV-A7, while diosmin interacted with R39, Q42, H40, L127, S128, T142, C147, H161, and I162. In

addition, both compounds were tested for inhibitory activity in RD cell infection with EV-A71 and CV-A16 3Cpro. The results showed that EGCG and diosmin could inhibit EV-A71 and CV-A16 while having no toxicity for RD cells. Moreover, the MD simulation analysis revealed that EGCG had a higher binding affinity than diosmin, supported by significantly lower SIE binding free energies, a higher number of contact atoms, and a higher number of key binding residues similar to rupintrivir. We suggest that EGCG and diosmin could be developed as the anti-HFMD agent.



APPENDIX
CHAPTER I
MANUSCRIPT I

Computational Screening of Newly Designed Compounds Against Coxsackievirus
A16 and Enterovirus A71

Amita Sripattaraphan¹, Kamonpan Sanachai¹, Warinthorn Chavasiri², Siwaporn Boonyasuppayakorn³ Phorn-phimon Maitarad⁴ and Thanyada Rungrotmongkol^{1,5, *}

¹ Structural and Computational Biology Research Unit, Department of Biochemistry, Faculty of Science, Chulalongkorn University, Bangkok, Thailand; bbeemita@gmail.com (A.S.); sanachaikamonpan@gmail.com (K.S.)

² Department of Chemistry, Faculty of Science, Chulalongkorn University, Bangkok 10330, Thailand; warinthorn.c@chula.ac.th

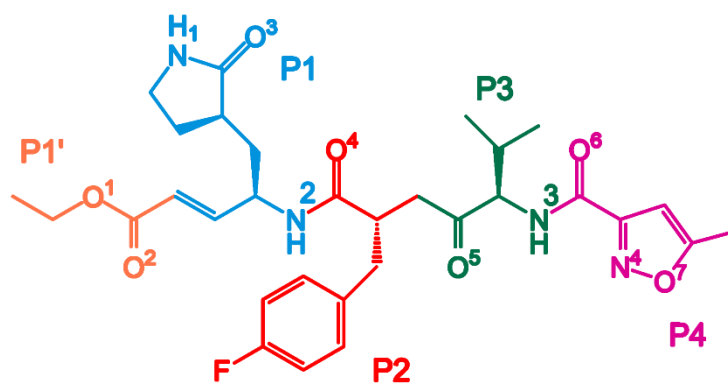
³ Applied Medical Virology Research Unit, Department of Microbiology, Faculty of Medicine, Chulalongkorn University, Bangkok 10330, Thailand; siwaporn.b@chula.ac.th

⁴ Research Center of Nano Science and Technology, Shanghai University, Shanghai 200444, PR; pmaitarad@shu.edu.cn

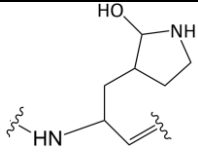
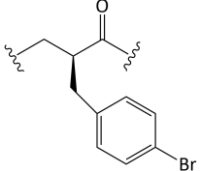
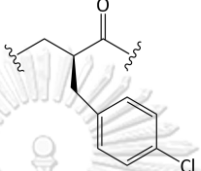
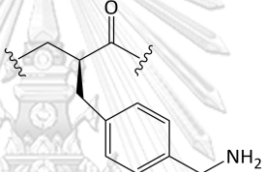
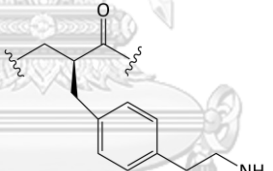
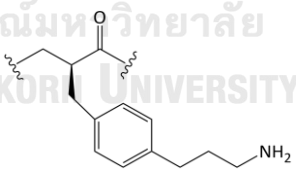
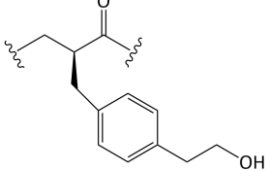
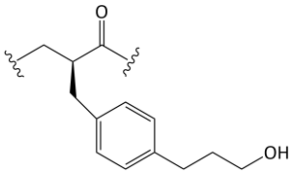
⁵ Ph.D. Program in Bioinformatics and Computational Biology, Graduate School, Chulalongkorn University, Bangkok 10330, Thailand

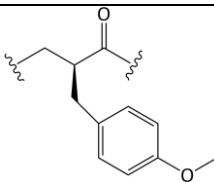
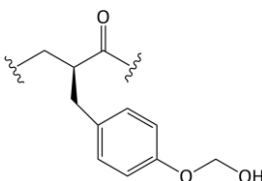
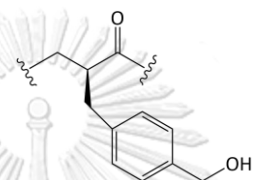
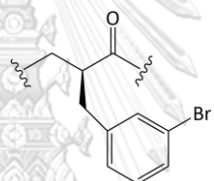
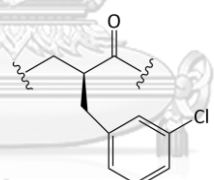
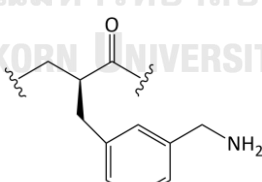
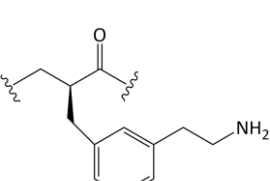
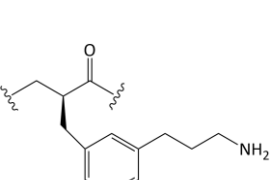
* Correspondence: thanyada.r@chula.ac.th, t.rungrotmongkol@gmail.com

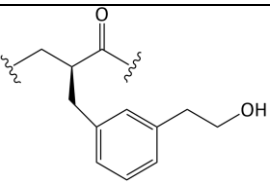
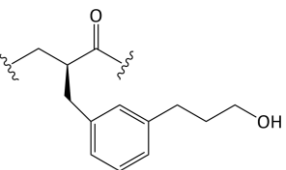
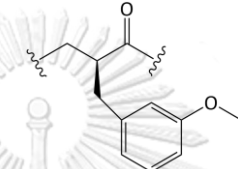
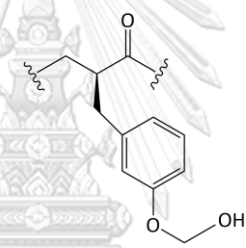
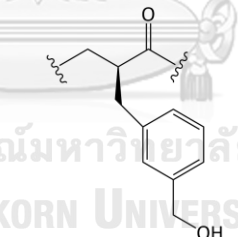
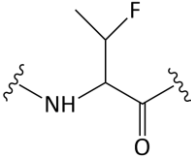
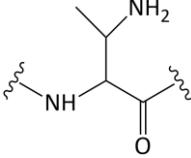
Table S1 Chemical structures of rupintrivir and its 50 analogs

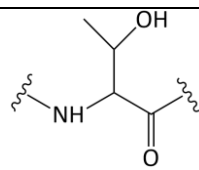
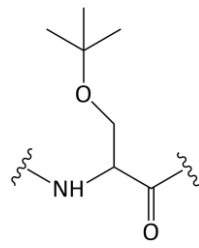
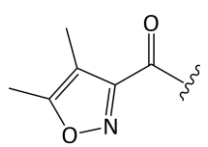
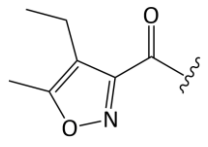
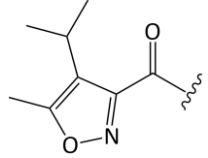
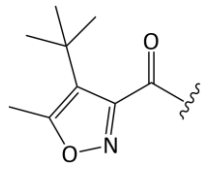
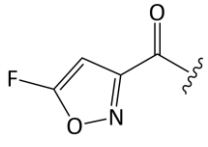
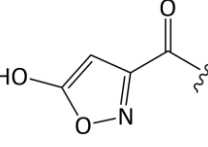


Code	P1'	P1	P2	P3	P4
rupintrivir					
P1'-1					
P1'-2					
P1-1					
P1-2					
P1-3					
P1-4					

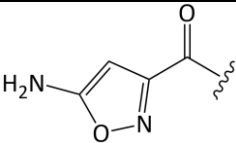
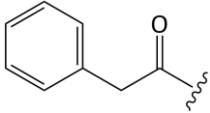
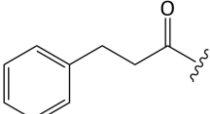
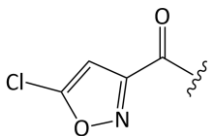
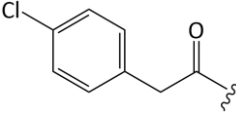
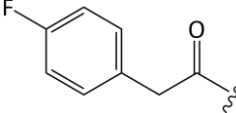
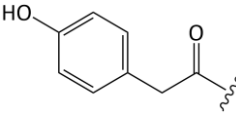
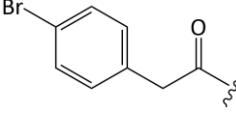
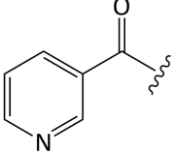
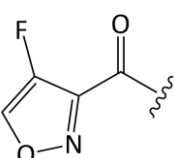
Code	P1'	P1	P2	P3	P4
P1-5					
P2-p1					
P2-p2					
P2-p3					
P2-p4					
P2-p5					
P2-p6					
P2-p7					

Code	P1'	P1	P2	P3	P4
P2-p8					
P2-p9					
P2-p10					
P2-m1					
P2-m2					
P2-m3					
P2-m4					
P2-m5					

Code	P1'	P1	P2	P3	P4
P2-m6					
P2-m7					
P2-m8					
P2-m9					
P2-m10					
P3-1					
P3-2					

Code	P1'	P1	P2	P3	P4
P3-3					
P3-4					
P4-1					
P4-2					
P4-3					
P4-4					
P4-5					
P4-6					



Code	P1'	P1	P2	P3	P4
P4-7					
P4-8					
P4-9					
P4-10					
P4-11					
P4-12					
P4-13					
P4-14					
P4-15					
P4-16					



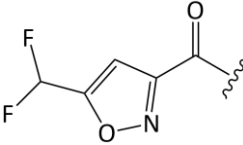
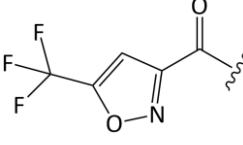
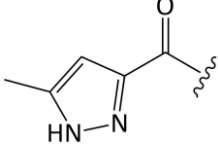
Code	P1'	P1	P2	P3	P4
P4-17					
P4-18					
P4-19					



Table S2 Binding free energy based on the MM/PB(GB)SA method of rupintrivir and P2-m3

Compound		EV-A71		CV-A16	
		MM/PBSA	MM/GBSA	MM/PBSA	MM/GBSA
Rupintrivir	Run1	-10.1±1.5	-11.9±0.6	-7.8±0.5	-9.5±0.8
	Run2	-7.1±1.2	-9.1±1.0	-6.0±0.4	-8.5±0.9
	Run3	-6.4±1.0	-8.6±0.7	-8.9±0.9	-11.1±1.2
	Mean±SD	-7.9±2.0	-9.9±1.4	-7.6±1.1	-9.7±1.7
P2-m3	Run1	-17.2±0.6	-17.4±0.5	-11.8±0.3	-13.0±0.4
	Run2	-15.1±0.6	-15.6±0.3	-10.4±0.5	-12.7±0.3
	Run3	-15.0±0.8	-15.4±0.6	-10.1±0.7	-12.9±1.0
	Mean±SD	-15.8±1.2	-16.1±0.8	-10.8±0.9	-12.9±1.1

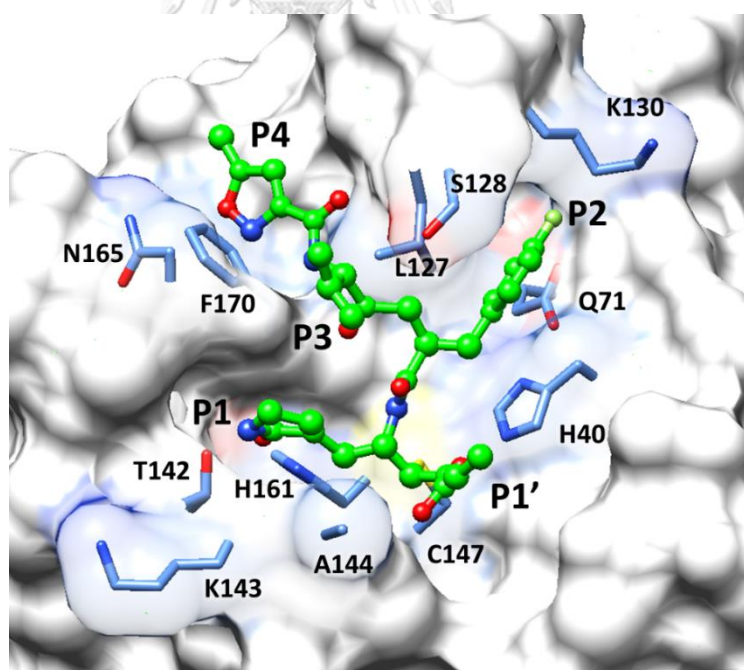


Fig. S1 Rupintrivir (bond and stick model) binding at the active site of EV-A71 3Cpro, where its the surrounding residues (stick model) are shown and labeled

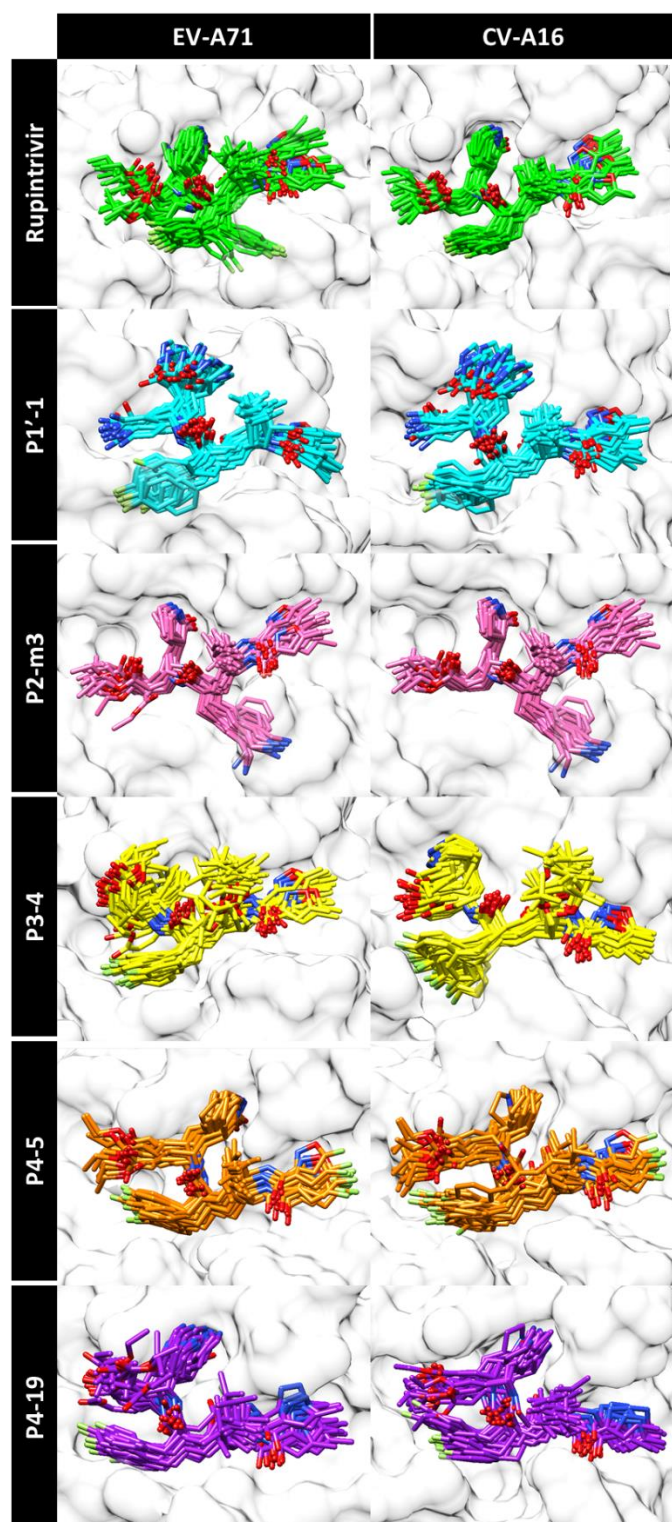


Fig. S2 Superimposition of rupintrivir and 5 screened analogs at the binding pocket of EV-A71 and CV-A16 3Cpro derived from the last 50 ns of run1 MD simulation

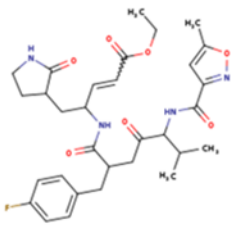
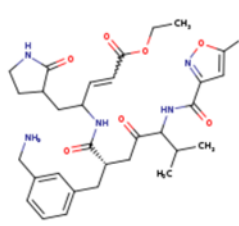
Compound	Solubility
 <p>Rupintrivir</p>	Log S (ESOL) [?] -6.05 Solubility 5.36e-04 mg/ml ; 8.95e-07 mol/l Class [?] Poorly soluble
 <p>P2-m3 analog</p>	Log S (ESOL) [?] -3.72 Solubility 1.17e-01 mg/ml ; 1.92e-04 mol/l Class [?] Soluble

Fig S3. The solubility from ADMET property of rupintrivir and P2-m3. P2-m3 showed better solubility than rupintrivir

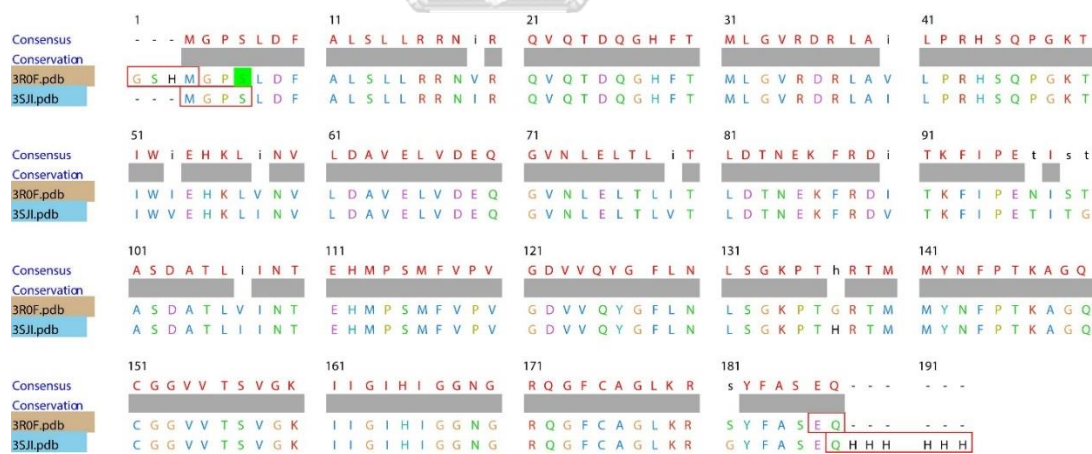


Fig S4. Sequence alignment of EV-A71 (PDB code: 3SJI) and CV-A16 (PDB code: 3R0F) proteases

CHAPTER II

MANUSCRIPT II

Discovery of potent compounds for active against coxsackievirus A16 and
enterovirus A71 by virtual screening

Amita Sripattarphan¹, Kamonpan Sanachai¹, Siwaporn Boonyasuppayakorn²,
Warinthorn Chavasiri³, Peter Wolschann^{4,5}, Thierry Langer⁴, Phornphimon Maitarad⁶,
Thanyada Rungrotmongkol^{1,7*}

¹ Structural and Computational Biology Research Unit, Department of Biochemistry, Faculty of Science, Chulalongkorn University, Bangkok, Thailand

² Applied Medical Virology Research Unit, Department of Microbiology, Faculty of Medicine, Chulalongkorn University, Bangkok 10330, Thailand

³ Department of Chemistry, Faculty of Science, Chulalongkorn University, Bangkok 10330, Thailand

⁴ Department of Pharmaceutical Chemistry, Faculty of Life Sciences, University of Vienna, Althanstraße 14, A-1090 Vienna, Austria

⁵ Institute of Theoretical Chemistry, University of Vienna, Vienna 1090, Austria

⁶ Research Center of Nano Science and Technology, Shanghai University, Shanghai 200444, PR

⁷ Ph.D. Program in Bioinformatics and Computational Biology, Faculty of Science, Chulalongkorn University, Bangkok 10330, Thailand

* Correspondence: thanyada.r@chula.ac.th, t.rungrotmongkol@gmail.com

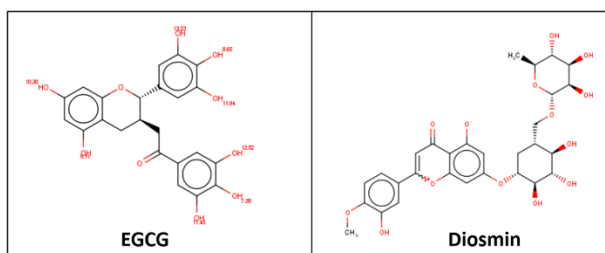


Fig S1. Sequence alignment of EV-A71 (PDB code: 3SJ1) and CV-A16 (PDB code: 3R0F) proteases

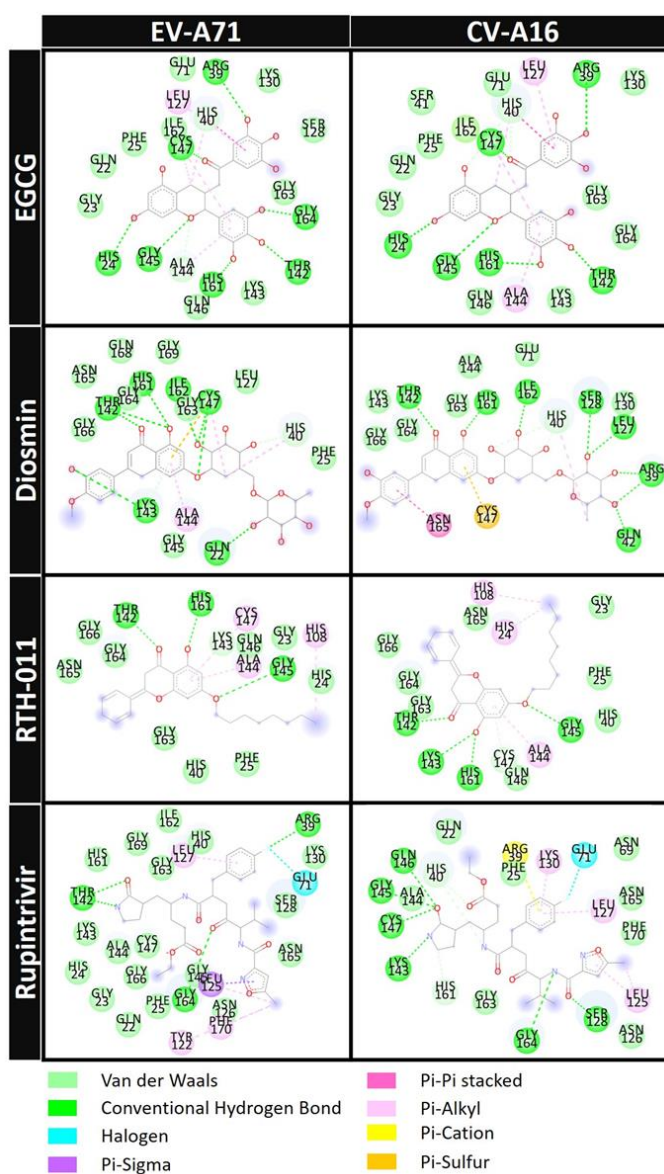


Fig S2. 2D interactions of potent compounds and rupintrivir in EV-A71 and CV-A16 3Cpro complexes

Table S1. The cytotoxicity, inhibitory activity and selective index of diosmin and EGCG toward RD cell infection by EV-A71 and CV-A16.

Compounds	CC ₅₀	EV-A71		CV-A16	
		EC ₅₀	SI	EC ₅₀	SI
Diosmin	>500	21.02±1.57µM	23.80	30.68±3.25 µM	16.30
EGCG	>250	12.86±1.30 µM	20.89	15.54±1.50 µM	16.08
Rupintrivir	>100	47.33±8.04nM	2112.97	49.33±7.3 nM	2027.0



REFERENCES

1. Manila, W.H.O.R.O.f.W.P., *A guide to clinical management and public health response for hand, foot and mouth disease (HFMD)*. 2011, Manila: WHO Regional Office for Western Pacific.
 2. Lu, G., et al., *Enterovirus 71 and coxsackievirus A16 3C proteases: binding to rupintrivir and their substrates and anti-hand, foot, and mouth disease virus drug design*. *J Virol*, 2011. **85**(19): p. 10319-31.
 3. Sarma, N., *Hand, foot, and mouth disease: current scenario and Indian perspective*. *Indian J Dermatol Venereol Leprol*, 2013. **79**(2): p. 165-75.
 4. Guerra, A.M., E. Orille, and M. Waseem, *Hand Foot And Mouth Disease*, in *StatPearls*. 2022, StatPearls Publishing
- Copyright © 2022, StatPearls Publishing LLC.: Treasure Island (FL).
5. Omaña-Cepeda, C., et al., *A literature review and case report of hand, foot and mouth disease in an immunocompetent adult*. *BMC research notes*, 2016. **9**: p. 165-165.
 6. Tsai, M.-T., et al., *Real-time monitoring of human enterovirus (HEV)-infected cells and anti-HEV 3C protease potency by fluorescence resonance energy transfer*. *Antimicrobial agents and chemotherapy*, 2009. **53**(2): p. 748-755.
 7. Cox, B. and F. Levent, *Hand, Foot, and Mouth Disease*. *JAMA*, 2018. **320**(23): p. 2492-2492.
 8. Tsai, M.T., et al., *Real-time monitoring of human enterovirus (HEV)-infected cells and anti-HEV 3C protease potency by fluorescence resonance energy transfer*. *Antimicrob Agents Chemother*, 2009. **53**(2): p. 748-55.
 9. Zhang, X., et al., *Rupintrivir is a promising candidate for treating severe cases of enterovirus-71 infection: evaluation of antiviral efficacy in a murine infection model*. *Antiviral Res*, 2013. **97**(3): p. 264-9.
 10. Wang, J., Y. Hu, and M. Zheng, *Enterovirus A71 antivirals: Past, present, and future*. *Acta Pharmaceutica Sinica B*, 2022. **12**(4): p. 1542-1566.
 11. Wang, J., et al., *Crystal structures of enterovirus 71 3C protease complexed with*

- rupintrivir reveal the roles of catalytically important residues.* J Virol, 2011. **85**(19): p. 10021-30.
12. Matthews, D.A., et al., *Structure-assisted design of mechanism-based irreversible inhibitors of human rhinovirus 3C protease with potent antiviral activity against multiple rhinovirus serotypes.* Proc Natl Acad Sci U S A, 1999. **96**(20): p. 11000-7.
 13. Kuo, C.-J., et al., *Design, synthesis, and evaluation of 3C protease inhibitors as anti-enterovirus 71 agents.* Bioorganic & medicinal chemistry, 2008. **16**(15): p. 7388-7398.
 14. Wang, Y., et al., *Structure of the Enterovirus 71 3C Protease in Complex with NK-1.8k and Indications for the Development of Antienterovirus Protease Inhibitor.* Antimicrobial agents and chemotherapy, 2017. **61**(7): p. e00298-17.
 15. Hildebrand, P.W., A.S. Rose, and J.K.S. Tiemann, *Bringing Molecular Dynamics Simulation Data into View.* Trends Biochem Sci, 2019. **44**(11): p. 902-913.
 16. Samanta, A. and D. S., *Roles of Flavonoids in Plants.* International Journal of Pharmaceutical Science and Technology, 2011. **6**: p. 12-35.
 17. Panche, A.N., A.D. Diwan, and S.R. Chandra, *Flavonoids: an overview.* Journal of Nutritional Science, 2016. **5**: p. e47.
 18. Khachatoorian, R., et al., *Divergent antiviral effects of bioflavonoids on the hepatitis C virus life cycle.* Virology, 2012. **433**(2): p. 346-355.
 19. Li, S., T. Hattori, and E.N. Kodama, *Epigallocatechin gallate inhibits the HIV reverse transcription step.* Antivir Chem Chemother, 2011. **21**(6): p. 239-43.
 20. Moghaddam, E., et al., *Baicalin, a metabolite of baicalein with antiviral activity against dengue virus.* Sci Rep, 2014. **4**: p. 5452.
 21. Haggag, Y.A., N.E. El-Ashmawy, and K.M. Okasha, *Is hesperidin essential for prophylaxis and treatment of COVID-19 Infection?* Medical Hypotheses, 2020. **144**: p. 109957.
 22. Kurogi, Y. and O.F. Güner, *Pharmacophore modeling and three-dimensional database searching for drug design using catalyst.* Curr Med Chem, 2001. **8**(9): p. 1035-55.
 23. Liu, C., et al., *Pharmacophore-Based Virtual Screening Toward the Discovery of Novel Anti-echinococcal Compounds.* Frontiers in Cellular and Infection

- Microbiology, 2020. **10**.
24. Shin, W.J. and B.L. Seong, *Recent advances in pharmacophore modeling and its application to anti-influenza drug discovery*. Expert Opin Drug Discov, 2013. **8**(4): p. 411-26.
 25. Yang, S.Y., *Pharmacophore modeling and applications in drug discovery: challenges and recent advances*. Drug Discov Today, 2010. **15**(11-12): p. 444-50.
 26. Zhu, R.-n., et al., *[Study on the association of hand, foot and mouth disease and enterovirus 71/CA16 among children in Beijing, 2007]*. Zhonghua liu xing bing xue za zhi = Zhonghua liuxingbingxue zazhi, 2007. **28**(10): p. 1004-1008.
 27. Sano, T., et al., *Temporal and geographical clustering of Kawasaki disease in Japan: 2007-2012*. Pediatr Int, 2016. **58**(11): p. 1140-1145.
 28. Huang, K.Y., et al., *Enterovirus 71 in Taiwan, 2004-2006: epidemiological and virological features*. Scand J Infect Dis, 2008. **40**(6-7): p. 571-4.
 29. Chan, K.P., et al., *Epidemic hand, foot and mouth disease caused by human enterovirus 71, Singapore*. Emerg Infect Dis, 2003. **9**(1): p. 78-85.
 30. Puenpa, J., et al., *Hand, foot, and mouth disease caused by coxsackievirus A6, Thailand, 2012*. Emerging infectious diseases, 2013. **19**(4): p. 641-643.
 31. da Silva, E.E., M.T. Winkler, and M.A. Pallansch, *Role of enterovirus 71 in acute flaccid paralysis after the eradication of poliovirus in Brazil*. Emerging infectious diseases, 1996. **2**(3): p. 231-233.
 32. Long, L., et al. *Neurological complications and risk factors of cardiopulmonary failure of EV-A71-related hand, foot and mouth disease*. Scientific reports, 2016. **6**, 23444 DOI: 10.1038/srep23444.
 33. Ooi, M.H., et al., *Clinical features, diagnosis, and management of enterovirus 71*. Lancet Neurol, 2010. **9**(11): p. 1097-105.
 34. Patick, A.K., et al., *In vitro antiviral activity of AG7088, a potent inhibitor of human rhinovirus 3C protease*. Antimicrob Agents Chemother, 1999. **43**(10): p. 2444-50.
 35. Lee, J.C., et al., *A mammalian cell-based reverse two-hybrid system for functional analysis of 3C viral protease of human enterovirus 71*. Anal Biochem, 2008. **375**(1): p. 115-23.

36. Binford, S.L., et al., *Conservation of amino acids in human rhinovirus 3C protease correlates with broad-spectrum antiviral activity of rupintrivir, a novel human rhinovirus 3C protease inhibitor*. *Antimicrob Agents Chemother*, 2005. **49**(2): p. 619-26.
37. Hayden, F.G., et al., *Phase II, randomized, double-blind, placebo-controlled studies of rupintrivir nasal spray 2-percent suspension for prevention and treatment of experimentally induced rhinovirus colds in healthy volunteers*. *Antimicrob Agents Chemother*, 2003. **47**(12): p. 3907-16.
38. Schmidt, N.J., E.H. Lennette, and H.H. Ho, *An apparently new enterovirus isolated from patients with disease of the central nervous system*. *J Infect Dis*, 1974. **129**(3): p. 304-9.
39. Sun, L., et al., *Antiviral Activity of Broad-Spectrum and Enterovirus-Specific Inhibitors against Clinical Isolates of Enterovirus D68*. *Antimicrobial agents and chemotherapy*, 2015. **59**(12): p. 7782-7785.
40. Dragovich, P.S., et al., *Structure-Based Design, Synthesis, and Biological Evaluation of Irreversible Human Rhinovirus 3C Protease Inhibitors. 2. Peptide Structure–Activity Studies*. *Journal of Medicinal Chemistry*, 1998. **41**(15): p. 2819-2834.
41. Lacroix, C., et al., *The enterovirus 3C protease inhibitor SG85 efficiently blocks rhinovirus replication and is not cross-resistant with rupintrivir*. *Antimicrobial agents and chemotherapy*, 2015. **59**(9): p. 5814-5818.
42. Jetsadawisut, W., et al., *Susceptibility of inhibitors against 3C protease of coxsackievirus A16 and enterovirus A71 causing hand, foot and mouth disease: A molecular dynamics study*. *Biophys Chem*, 2016. **219**: p. 9-16.
43. Bleiziffer, P., K. Schaller, and S. Riniker, *Machine Learning of Partial Charges Derived from High-Quality Quantum-Mechanical Calculations*. *Journal of Chemical Information and Modeling*, 2018. **58**(3): p. 579-590.
44. Olsson, M.H.M., et al., *PROPKA3: Consistent Treatment of Internal and Surface Residues in Empirical pKa Predictions*. *Journal of Chemical Theory and Computation*, 2011. **7**(2): p. 525-537.
45. Case, D.A., et al., *The Amber biomolecular simulation programs*. *J Comput*

- Chem, 2005. **26**(16): p. 1668-88.
46. Frisch, M.J. *Gaussian09*. 2009; Available from: <http://www.gaussian.com/>.
 47. Mackerell, A.D., Jr., *Empirical force fields for biological macromolecules: overview and issues*. J Comput Chem, 2004. **25**(13): p. 1584-604.
 48. Case, D.A., et al., *AMBER16*. 2016.
 49. Sousa da Silva, A.W. and W.F. Vranken, *ACPYPE - AnteChamber PYthon Parser interfacE*. BMC Res Notes, 2012. **5**: p. 367.
 50. Wang, J., et al., *Development and testing of a general amber force field*. J Comput Chem, 2004. **25**(9): p. 1157-74.
 51. Jorgensen, W.L., et al., *Comparison of simple potential functions for simulating liquid water*. The Journal of chemical physics, 1983. **79**(2): p. 926-935.
 52. Wittayanarakul, K., et al., *Insights into Saquinavir Resistance in the G48V HIV-1 Protease: Quantum Calculations and Molecular Dynamic Simulations*. Biophysical Journal, 2005. **88**(2): p. 867-879.
 53. Maier, J.A., et al., *ff14SB: Improving the Accuracy of Protein Side Chain and Backbone Parameters from ff99SB*. Journal of Chemical Theory and Computation, 2015. **11**(8): p. 3696-3713.
 54. Roe, D.R. and T.E. Cheatham, 3rd, *PTRAJ and CPPTRAJ: Software for Processing and Analysis of Molecular Dynamics Trajectory Data*. J Chem Theory Comput, 2013. **9**(7): p. 3084-95.
 55. Knapp, B., et al., *Is an intuitive convergence definition of molecular dynamics simulations solely based on the root mean square deviation possible?* Journal of computational biology : a journal of computational molecular cell biology, 2011. **18**(8): p. 997-1005.
 56. Meng, X.-D., et al. *Epidemical and etiological study on hand, foot and mouth disease following EV-A71 vaccination in Xiangyang, China*. Scientific reports, 2020. **10**, 20909 DOI: 10.1038/s41598-020-77768-7.
 57. Xing, W., et al., *Hand, foot, and mouth disease in China, 2008-12: an epidemiological study*. Lancet Infect Dis, 2014. **14**(4): p. 308-318.
 58. Binford, S.L., et al., *In vitro resistance study of rupintrivir, a novel inhibitor of human rhinovirus 3C protease*. Antimicrobial agents and chemotherapy, 2007.

- 51**(12): p. 4366-4373.
59. Gordon, O., et al., *Silver coordination polymers for prevention of implant infection: thiol interaction, impact on respiratory chain enzymes, and hydroxyl radical induction*. *Antimicrobial agents and chemotherapy*, 2010. **54**(10): p. 4208-4218.
60. Bachmetov, L., et al., *Suppression of hepatitis C virus by the flavonoid quercetin is mediated by inhibition of NS3 protease activity*. *J Viral Hepat*, 2012. **19**(2): p. e81-8.
61. Lu, N., R. Khachatourian, and S.W. French, *Quercetin: bioflavonoids as part of interferon-free hepatitis C therapy?* *Expert Rev Anti Infect Ther*, 2012. **10**(6): p. 619-21.
62. Kim, N.D., et al., *Discovery of novel HCV polymerase inhibitors using pharmacophore-based virtual screening*. *Bioorg Med Chem Lett*, 2011. **21**(11): p. 3329-34.
63. Beisen, S., et al., *KNIME-CDK: Workflow-driven cheminformatics*. *BMC Bioinformatics*, 2013. **14**(1): p. 257.
64. Wolber, G. and T. Langer, *LigandScout: 3-D Pharmacophores Derived from Protein-Bound Ligands and Their Use as Virtual Screening Filters*. *Journal of Chemical Information and Modeling*, 2005. **45**(1): p. 160-169.
65. Hengphasatporn, K., et al., *Multiple Virtual Screening Strategies for the Discovery of Novel Compounds Active Against Dengue Virus: A Hit Identification Study*. *Scientia Pharmaceutica*, 2020. **88**(1).
66. Fawcett, T., *An introduction to ROC analysis*. *Pattern Recognition Letters*, 2006. **27**(8): p. 861-874.
67. ChemAxon, *MarvinSketch*. 2018.
68. Yepes-Pérez, A.F., et al., *Investigating Potential Inhibitory Effect of Uncaria tomentosa (Cat's Claw) against the Main Protease 3CL(pro) of SARS-CoV-2 by Molecular Modeling*. *Evid Based Complement Alternat Med*, 2020. **2020**: p. 4932572.
69. Boonyasuppayakorn, S., et al., *Simplified dengue virus microwell plaque assay*

- using an automated quantification program. *J Virol Methods*, 2016. **237**: p. 25-31.
70. Tan, J., et al., *3C protease of enterovirus 68: structure-based design of Michael acceptor inhibitors and their broad-spectrum antiviral effects against picornaviruses*. *Journal of virology*, 2013. **87**(8): p. 4339-4351.
71. Wermuth, C.G., et al., *Glossary of terms used in medicinal chemistry (IUPAC Recommendations 1998)*. *Pure and Applied Chemistry*, 1998. **70**(5): p. 1129-1143.
72. Sripattaraphan, A., et al., *Computational Screening of Newly Designed Compounds against Coxsackievirus A16 and Enterovirus A71*. *Molecules (Basel, Switzerland)*, 2022. **27**(6): p. 1908.
73. Wieder, M., et al., *Common Hits Approach: Combining Pharmacophore Modeling and Molecular Dynamics Simulations*. *Journal of Chemical Information and Modeling*, 2017. **57**(2): p. 365-385.
74. Opo, F.A.D.M., et al., *Structure based pharmacophore modeling, virtual screening, molecular docking and ADMET approaches for identification of natural anti-cancer agents targeting XIAP protein*. *Scientific Reports*, 2021. **11**(1): p. 4049.
75. Wang, J., et al., *Inhibition of Enterovirus 71 Replication by 7-Hydroxyflavone and Diisopropyl-Flavon7-yl Phosphate*. *PLOS ONE*, 2014. **9**(3): p. e92565.
76. Wang, J., et al., *Anti-Enterovirus 71 Effects of Chrysin and Its Phosphate Ester*. *PLOS ONE*, 2014. **9**(3): p. e89668.
77. Yao, C., et al., *Inhibition of enterovirus 71 replication and viral 3C protease by quercetin*. *Virology journal*, 2018. **15**(1): p. 116-116.
78. Zhang, W., et al., *Apigenin inhibits enterovirus-71 infection by disrupting viral RNA association with trans-acting factors*. *PLoS One*, 2014. **9**(10): p. e110429.
79. Carneiro, B.M., et al., *The green tea molecule EGCG inhibits Zika virus entry*. *Virology*, 2016. **496**: p. 215-218.
80. Huan, C., et al., *Epigallocatechin-3-Gallate, the Main Polyphenol in Green Tea, Inhibits Porcine Epidemic Diarrhea Virus In Vitro*. *Frontiers in Pharmacology*, 2021. **12**.

81. Song, J.M., K.H. Lee, and B.L. Seong, *Antiviral effect of catechins in green tea on influenza virus*. *Antiviral Res*, 2005. **68**(2): p. 66-74.





จุฬาลงกรณ์มหาวิทยาลัย
CHULALONGKORN UNIVERSITY

VITA

NAME Amita Sripattaraphan

DATE OF BIRTH 16 July 1995

PLACE OF BIRTH Nakhon Pathom

INSTITUTIONS ATTENDED Silapakorn University

HOME ADDRESS 29/1 Moo7, Nongpaklong, Muang, Nakhon pathom 73000

PUBLICATION Sripattaraphan, A., Sanachai, K., Chavasiri, W., Boonyasuppayakorn, S., Maitarad, P., & Rungrotmongkol, T. (2022). Computational Screening of Newly Designed Compounds against Coxsackievirus A16 and Enterovirus A71. *Molecules*, 27(6), 1908.